J. Fluid Mech. (1970), *vol.* 41, *part* 2, *pp.* 283–325
Boeing Symposium on Turbulence

Large-scale motion in the intermittent region of a turbulent boundary layer

By LESLIE S. G. KOVASZNAY, VALDIS KIBENS† AND RON F. BLACKWELDER

Department of Mechanics, The Johns Hopkins University

(Received 11 September 1969)

The outer intermittent region of a fully developed turbulent boundary layer with zero pressure gradient was extensively explored in the hope of shedding some light on the shape and motion of the interface separating the turbulent and non-turbulent regions as well as on the nature of the related large-scale eddies within the turbulent regime. Novel measuring techniques were devised, such as conditional sampling and conditional averaging, and others were turned to new uses, such as reorganizing in map form the space-time auto- and cross-correlation data involving both the U and V velocity components as well as I, the intermittency function. On the basis of the new experimental results, a conceptual model for the development of the interface and for the entrainment of new fluid is proposed.

1. Introduction

The curious fact that turbulent shear flows exhibit a sharp interface between the turbulent interior and the non-turbulent exterior has been known for a long time. Hot-wire probe signals clearly showing intermittency were first reported by Corrsin (1943) and later more extensive studies were carried out by Corrsin & Kistler (1955) as well as many others. Besides the hot-wire anemometer techniques, others, mainly optical, have also been reported. Fiedler & Head (1966) rendered the turbulent regime visible by injecting smoke and by using appropriate lighting. They obtained quantitative information on at least some of the statistical properties of the intermittent region. Theoretical efforts are less numerous. Corrsin & Kistler (1955) have attempted to estimate the rate of entrainment through the interface from the known properties of the turbulent fluctuations inside. Townsend (1966) has proposed a visco-elastic model for the motion of the interface.

At the outset of the experimental programme reported here the authors were convinced that new experimental techniques were necessary in order to obtain more revealing details. With the introduction of conditional sampling and conditional averaging, the measurement of new statistical properties became feasible. On one hand the difference between the turbulent and non-turbulent zones became clearly discernable by 'zone averaging'; on the other hand, with

† Present address: Department of Aerospace Engineering, University of Michigan.

Printed in Great Britain

the measurement of 'point average' values, the distribution of flow properties across the interface were obtained. During the course of the work it became more and more apparent that the interrelation between the motion of the interface and the large-scale fluctuations inside the fully turbulent boundary layer is quite important so new methods were devised to study the large-scale structure of the flow, both in the intermittent and in the fully turbulent regime. The measurement of space-time correlation, a technique well established by Favre, Gaviglio & Dumas (1957, 1958, 1967), was utilized here, but with a new emphasis and a new form of presentation. Furthermore, it was felt that space-time correlations taken with large streamwise separation of the probes can serve as a means to suppress the contribution from the small-scale eddies, so the auto-correlation and cross-correlation maps prepared this way will show the 'lasting' properties of the large-scale motion. These maps involve the flow variables, u, v and I, the latter being the intermittency function indicating the local (turbulent or non-turbulent) state of the flow. The maps clearly show the areas of positive and negative correlation and the locations of maxima and minima, so that the convection velocity of the turbulence pattern can be inferred. In addition, the distribution of iso-correlation contours around the peaks outline a gross pattern that can suggest models for the large eddies.

Correlation data can always be Fourier transformed into a spectral representation, but here that approach was not followed, quite deliberately, because it was felt that the important and rather striking spatial relationships become obscured by spectral representation. One, but by no means unique, model of the flow can be constructed from the correlation data, following a theory of Rice (1944, 1945), by regarding the physical phenomenon as the sum of identical functions (turbulent bursts) that arise at random, then travel with the appropriate convection velocity and slowly decay. These individual bursts then can be described deterministically although their aggregate is a stationary random function. It appears that such a representation is more adequate than a travelling wave model suggested by several authors.

The experimental data presented here was taken over a period of nearly 2 years. A portion of the conditional sampled data is contained in Kibens (1968), but is included here as it is a part of the complete picture not given elsewhere.

The hot-wire signals were processed entirely by analogue methods, mainly because wind tunnel time was inexpensive in comparison with available digital computers. This way much larger samples were processed, an advantage in the early exploratory phase of the research. Direct, 'on-line' digital data processing is possible; such an approach was followed by Kaplan & Laufer (1968).

2. Conditional sampling and conditional averaging

The output of a hot-wire probe placed in the outer region of a turbulent boundary layer has a characteristically 'intermittent' appearance, as two distinct types of signal appear to be alternating in a random sequence. One can be described intuitively as being turbulent and the other as non-turbulent. Corrsin & Kistler (1955) have observed that the vorticity fluctuation level is very small in

the non-turbulent regions of a boundary layer, but becomes quite large inside the turbulent bursts. Since there appears to be clearly two distinct states, one is immediately tempted to define an intermittency function $I(x, y, z, t)$ so that

$$I(x, y, z, t) = \begin{cases} 1 \text{ for turbulent flow,} \\ 0 \text{ for non-turbulent flow.} \end{cases}$$

The time average value of $I(x, y, z, t)$ is the intermittency factor, γ, which gives the fraction of the time that the probe spends in turbulent flow:

$$\gamma = \bar{I} \equiv \lim_{t_0 \to \infty} \frac{1}{t_0} \int_{t_1}^{t_1+t_0} I(t)\, dt. \tag{1}$$

The intermittency function I at a point is a random square wave and the instants when it changes from 0 to 1 and from 1 to 0 represent the condition that the turbulent non-turbulent interface is at the turbulence detector probe. Since it is assumed here that the interface is a continuously curved surface that separates the two types of flow, for a fixed observer there are two types of transitio ns One is when the probe enters the turbulent regime and these will be labelled 'Front'. The other is when the probe leaves the turbulent regime, and these will be labelled 'Back'.

It is clear to the experimenter that, in attempting to determine the intermittency function of I, there will be always some arbitrariness in the definition, so details of the actual method used are given in the appendix. It may be suggested here that, in order to define the interface, one faces the same type of difficulties as in defining the shore line of the sea; it always depends on the magnification, if you like, on the coarseness of the method of detection. The shoreline, on the one hand, may be considered relatively smooth, or, on the other hand, full of small inlets and islands, depending upon how small details are taken into account. Nevertheless, if one assumes that $I(x, y, z, t)$ can be suitably defined, it becomes possible to define other new kinds of averages.

If $Q(t)$ is a fluctuating quantity, (e.g. a velocity component at a given point), then the 'conventional time average', denoted here by a bar, is given by

$$\bar{Q} \equiv \lim_{t_0 \to \infty} \frac{1}{t_0} \int_{t_1}^{t_1+t_0} Q(t)\, dt. \tag{2}$$

Utilizing the intermittency function, $I(t)$, new conditional averages may be formed.

If $Q(t)$ is averaged only during the time intervals when $I(t) = 1$, this is termed a 'turbulent zone average':

$$\tilde{\bar{Q}} = \frac{\overline{IQ}}{\bar{I}} \equiv \lim_{t_0 \to \infty} \frac{1}{\gamma t_0} \int_{t_1}^{t_1+t_0} I(t) Q(t)\, dt. \tag{3}$$

Conversely, if $Q(t)$ is averaged only during the non-turbulent time intervals when $I(t) = 0$, the non-turbulent zone average is obtained

$$\tilde{\bar{Q}} = \frac{\overline{(1-I)Q}}{\overline{(1-I)}} \equiv \lim_{t_0 \to \infty} \frac{1}{(1-\gamma)t_0} \int_{t_1}^{t_1+t_0} [1 - I(t)] Q(t)\, dt. \tag{4}$$

The notation used for zone averages is as shown above, ($\overline{\sim}$) for the turbulent and ($\underset{\sim}{\sim}$) for the non-turbulent zone average. It is clear from the definition of (1), (2), (3) and (4) that the conventional average is the weighted average of the two zone averages

$$\bar{Q} = \gamma\overline{\tilde{Q}} + (1-\gamma)\underset{\sim}{\tilde{Q}}. \tag{5}$$

$Q(t)$ and $I(t)$, of course, do not need to be taken from the same point in space, and, in that case, the zone average will depend on the relative position of the detector probe located at x_0, y_0, z_0 giving $I(x_0, y_0, z_0, t)$ and the signal probe located at x, y, z giving $Q(x, y, z, t)$.

Another entirely different type of sampling and averaging can be constructed based on the instants when the interface passes over the detector probe. As mentioned above, one can distinguish here two kinds of transitions (Fronts and Backs). If the intermittency function $I(t)$ is differentiated with respect to time, a pulse train, consisting of positive and negative delta functions, results:

$$\dot{I}(t) \equiv \frac{\partial I}{\partial t} = (-1)^n \delta(t - t_n), \tag{6}$$

where each t_n is the instant of change in $I(t)$. For an even integer, $n = 2i$ and the monitor probe is entering the turbulent region (Front); for an odd integer, $n = 2i-1$ and the monitor probe is leaving the turbulent region (Back). The two pulse trains can be defined separately as $\hat{P}(t)$ and $\check{P}(t)$. For sampling at the 'Fronts',

$$2\hat{P}(t) \equiv \dot{I}(t) + |\dot{I}(t)| = \delta(t - t_{2i}). \tag{7}$$

For sampling at the 'Backs',

$$2\check{P}(t) \equiv -\dot{I}(t) + |\dot{I}(t)| = \delta(t - t_{2i-1}). \tag{8}$$

The conditional sampling of the continuous variable $Q(t)$ can now be performed and each pulse train of conditional samples can be represented as one of the two generalized functions of time:

$$\text{(Fronts)} \quad \hat{p}(t) = Q(t)\,\hat{P}(t), \tag{9}$$

and

$$\text{(Backs)} \quad \check{p}(t) = Q(t)\check{P}(t); \tag{10}$$

and the 'conditional point averages' can be defined as:

$$\hat{Q} \equiv \lim_{t_0 \to \infty} \frac{\int_{t_1}^{t_1+t_0} \hat{p}(t)\,dt}{\int_{t_1}^{t_1+t_0} \hat{P}(t)\,dt}, \tag{11}$$

$$\check{Q} \equiv \lim_{t_0 \to \infty} \frac{\int_{t_1}^{t_1+t_0} \check{p}(t)\,dt}{\int_{t_1}^{t_1+t_0} \check{P}(t)\,dt}. \tag{12}$$

All integrations are performed in the sense of generalized functions such as the Dirac delta function. In practice, of course, the pulse width used in the electronic

equipment will be finite but still small compared to the time intervals during which $Q(t)$ changes appreciably. The point average is in general a function of both sets of co-ordinates; x_0, y_0, z_0 and x, y, z.

It is reasonable to expect that for large separations of the two probes, the conditional point averages $\hat{Q}$ and $\check{Q}$ will revert to the conventional average, e.g.

$$\hat{Q}(x, y, z, x_0, y_0, z_0) \to \bar{Q}(x, y, z),$$

when

$$(x-x_0)^2+(y-y_0)^2+(z-z_0)^2 \to \infty,$$

because the temporal occurrence of the sampling pulse $\hat{P}(t)$ becomes statistically independent of the function $Q(t)$ being sampled.

As far as the function $Q(t)$ is concerned, it may be any flow variable, such as a velocity component, a velocity derivative or any square of the instantaneous velocity fluctuation; another is the instantaneous velocity product, such as the instantaneous value of the Reynolds stress.

The conditional point averaged turbulent velocity fluctuation level can be determined the following way. The signal $Q(t)$ is usually separated into the conventional average value and a fluctuation:

$$Q(t) = \bar{Q}+q(t), \quad \text{where} \quad \bar{q} = 0. \tag{13}$$

After having determined the conditional point average Q, and then subtracting it from the function $Q(t)$, the fluctuation $q_\wedge(t)$ around the conditional point average value becomes

$$q_\wedge(t) \equiv Q(t)-\hat{Q}. \tag{14}$$

From the definition, $\hat{q}_\wedge = 0$, but

$$\bar{q}_\wedge(t) = \bar{Q}-\hat{Q} \neq 0.$$

Forming the instantaneous square of $q_\wedge(t)$ and taking the conditional point average of that quantity, the conditionally averaged fluctuation level is then defined as

$$\hat{q}' \equiv [\hat{q}_\wedge^2]^{\frac{1}{2}}.$$

Zone averaged fluctuation intensities can be similarly defined. The qualities $\hat{q}'$, $\check{q}'$, $\tilde{\bar{q}}'$, $\bar{\tilde{q}}'$, etc., all approach the conventional r.m.s. value in the limit, when the conditional pulses from $I(t)$ or $\check{P}(t)$ etc. become statistically independent of $Q(t)$ (e.g. the detector probe and signal probe move far apart).

3. Space-time correlation

In order to obtain information on the large-scale motion and on its interrelation with the shape and motion of the turbulent non-turbulent interface, extensive space-time correlation measurements were taken. As mentioned earlier, measurements of space-time correlations was first pioneered by Favre *et al.* (1957, 1958, 1967), but later it was gradually adopted as a standard technique, especially by those interested in aerodynamically generated sound. Favre's group concentrated on measuring space-time auto-correlations of the

streamwise component of the turbulent velocity fluctuations, and has determined the effective convection velocity of the disturbances ('celerite' in French). Furthermore, with the use of the narrow band filtering, the phase velocity of the disturbances can be obtained. The present approach was quite different in two ways. First, space-time auto-correlation and cross-correlation measurements were taken involving several flow variables, u, v and I. Secondly, the space-time correlations were mapped out for relatively large separations in x and t in order to discover the large-scale or 'lasting' features of the turbulent field.

The co-ordinate system is defined as follows: x is positive in the downstream direction, parallel with the wall and with the free-stream velocity U_∞; y is normal to the wall, and z normal to both x and y. In the experiments one probe located at x_0, y_0, z_0 acquires the signal $P(t)$ and the other probe, located at x, y, z acquires the signal $Q(t)$. The time is also different as a relative time delay $t - t_0$ is introduced.

The space-time cross-correlation of P and Q is defined as

$$R_{PQ'} \equiv \frac{\overline{P(x_0, y_0, z_0, t_0)Q(x, y, z, t)}}{P'Q'}, \tag{15}$$

where the overbar represents time average and P' and Q' are the r.m.s. values of the functions P and Q.

If the functions P and Q are statistically homogeneous in space and stationary in time, the correlation $R_{PQ'}$ depends only on the difference in the co-ordinates $x - x_0$, $y - y_0$, $z - z_0$ and $t - t_0$. In a turbulent boundary layer with zero pressure gradient, the homogeneity with respect to z and stationarity with respect to t are expected. Since the growth of the boundary-layer thickness is slow, one may expect approximate homogeneity in x if the y co-ordinate is scaled with the local value of the boundary-layer thickness, but there is certainly no homogeneity in the y co-ordinate itself.

Here non-dimensional displacement co-ordinates are introduced:

$$X \equiv \frac{x - x_0}{\delta_0}; \quad Y \equiv \frac{y}{\delta} - \frac{y_0}{\delta_0}; \quad Z \equiv \frac{z - z_0}{\delta_0}; \quad T \equiv \frac{(t - t_0)U_\infty}{\delta_0}.$$

The boundary-layer thickness at $\delta_0 = \delta(x_0, z_0)$ and the free-stream velocity U_∞ were used for scaling except in Y, where scaling with the local value of δ is preferable so that $Y = 0$; for $y/\delta =$ constant. The correlation function is presented as

$$R_{PQ'}(X, Y, Z, T),$$

as a function of the four displacement co-ordinates, but, in addition, the value of y_0/δ_0 must be also specified. The experimental data will always be given in the form of three-dimensional iso-correlation surfaces or two-dimensional sections with iso-correlation contours. For a large value of T, the correlation will be small for all except around $X = U_c T$, $Y = 0$, $Z = 0$, but the actual shape and extent of the correlation pattern reveals the large-scale 'lasting' features of the flow. From a purely conceptual point of view, it would be preferable to choose a large but fixed value of T_0, then vary X, Y and Z and map out the contours of $R_{PQ'} =$ constant.

For experimental convenience, here an alternate method was chosen. It is somewhat similar to the method used by Kovasznay, Komoda & Vasudeva (1962). The value $X = X_0$ was held constant throughout an experiment and the separation co-ordinates Y, Z and T were varied. The convenience of available time-correlation measuring equipment made this choice almost imperative.

If the turbulence pattern was convected as a strictly 'frozen pattern' (Taylor's hypothesis) with a convection velocity U_c, then the two methods would of course yield exactly the same results. In that case,

$$Q(x, y, z, t) = Q_0(x - U_c t, y, z), \tag{16}$$

and

$$R_{QQ'}(X, Y, Z, T) = R_0(X - U_c T, Y, Z). \tag{17}$$

Taylor's hypothesis is only approximately valid so the correlations obtained with $X = X_0 =$ constant and by varying Y, Z and T are only qualitatively equivalent to those that would have been obtained with $T = T_0 =$ constant and varying X, Y and Z.

$$R_{QQ'}(X_0 + \tilde{X}, Y, Z, T_0) \approx R_{QQ'}(X_0, Y, Z, T_0 + \tilde{T}), \tag{18}$$

where

$$\tilde{X} = -U_c \tilde{T}. \tag{19}$$

Because of the negative sign, the corresponding correlation patterns would be approximate mirror images of each other

$$R_{QQ'}(\tilde{X}) \approx R_{QQ'}(-\tilde{T}U_c).$$

The space-time correlations involving the intermittency function I were also taken. Although $I(t)$ is a random square wave, the correlation map for $R_{II'}$ gives the average shape, convection velocity and decay of the interface pattern. Since the intermittency function I is either zero or unity, a good analogy can be imagined regarding the free surface of the ocean. If a local probe placed into the waves would indicate either 'Water' or 'Air', and the resulting random square wave would be acquired from two points, the space-time auto-correlation of I could be calculated. This would give information concerning the average shape, convection velocity and decay of the wave pattern.

Regarding $R_{II'}$ there is a further problem. It is convenient to form the correlation of two functions that each have separately a zero mean value. Therefore the correlation coefficient between I_1 and I_2 will be defined as that of

$$P = I_1 - \gamma_1, \quad Q = I_2 - \gamma_2,$$

so that

$$R_{I_1 I_2} \equiv \frac{\overline{(I_1 - \gamma_1)(I_2 - \gamma_2)}}{\overline{(I_1 - \gamma_1)'(I_2 - \gamma_2)'}}. \tag{20}$$

It needs to be mentioned here that the conditional averages may be regarded as a special form of correlation. In fact the zone averages are proportional to the cross-correlation between the function $Q(t)$ to be sampled and $I(t)$ or $1 - I(t)$. The point averages are proportional to cross-correlations of $Q(t)$ and $\hat{P}(t)$ or $\check{P}(t)$; but, since those are generalized function (pulse trains), it is preferrable to use a different terminology.

4. Equipment and experimental procedures

4.1. *Wind tunnel*

All measurements were taken in a low-speed wind tunnel at a nominal free-stream velocity $U_\infty = 430$ cm/sec. The tunnel is of open return type, driven by a centrifugal blower, followed first by a diffusor section, then a 420 cm wide, 360 cm high and 210 cm long settling chamber provided with seven fine mesh screens. After the settling chamber there is a two-dimensional contraction (7:1) in the vertical plane. The test section has a nominal width of 52 cm at the beginning of the nearly parallel working section. The height is 360 cm and it remains constant, and its total length is 1224 cm. At the end of the test section, the air discharges into the room.

The width of the channel is flared out somewhat in order to allow for boundary-layer growth so that at the downstream end at $x = 1224$ cm it reaches a width of about 55 cm. All the measurements were made on one wall that was built to be plane within $\pm 0{\cdot}0125$ cm over the entire length and height of the tunnel. At the location $x = 234$ cm, on each vertical wall a row of hemispherical head upholstery tacks (0·3 cm high) spaced at 3·5 cm apart, trip the boundary layer in order to obtain a well-stabilized turbulent layer. Most of the measurements reported here were taken at the nominal position $x = 900$ cm at a midsection station, where the conventional boundary-layer thickness was typically $\delta = 10$ cm ($y = \delta$ where $\overline{U}/U_\infty = 0{\cdot}99$).

It was observed that the boundary-layer thickness, as well as other gross properties, varied somewhat in the z or spanwise direction, and a rough spanwise periodicity with a period of approximately 25 cm was evident. After some experimentation, it was found that one of the most sensitive indicators of the spanwise variation is the intermittency factor $\gamma\,(y, z)$ measured at a fixed distance y_0 from the wall. The distance from the wall was chosen to be near the estimated half intermittency ($\gamma = 0{\cdot}5$) value. One spanwise region where most of the measurements were taken was chosen at $z = 150$ cm ($z = 0$ is the floor of the tunnel), where the intermittency factor for a fixed y was both constant and near its minimal value with respect to z.

Since measurements were taken over a period of more than a year, changes of general temperature conditions in the building (heating in winter, air conditioning in summer) slightly affected the density (temperature) stratification in the room; consequently, there was some shifting of the spanwise (vertical) pattern. In order to minimize this effect, the results of each run were normalized with respect to δ, the conventional boundary-layer thickness, and U_∞, the free-stream velocity (measured at $y = 2\delta$).

Since the dynamic pressure corresponding to the free-stream velocity was only about 0·1 cm H_2O, the static pressure distribution along the centreline of the tunnel cannot be measured with sufficient accuracy, so, instead, the free-stream velocity distribution was measured using a 'vortex-shedding' probe. This operates by counting the number of vortices shed in a given period (typically a 50 sec period) from a cylinder of small diameter ($d = 0{\cdot}033$ cm) chosen, so

that the Reynolds number was always within the purely periodic range:

$$50 \leqslant \frac{U_\infty d}{\nu} \leqslant 100.$$

Then the shedding frequency was converted to velocity by using an empirical relationship originally suggested by Roshko (1953) and later improved upon by Tritton (1959).

4.2. *Hot-wire anemometers*

Constant temperature hot-wire anemometers with linearizers were used as first described by Kovasznay, Miller & Vasudeva (1963). In the later phases of the work, the more stable linearizers described by Kovasznay & Chevray (1969) replaced the original ones. Tungsten sires of 3·8 micron diameter were used for all hot-wire probes. The wires were partially copper plated, leaving an active bare section of 0·2 cm length, then were soft-soldered to the tips of jeweller's broaches. The output voltage of the linearizer was set typically to 2·5 V, always corresponding to the free-stream velocity U_∞. The frequency response of the entire hot-wire equipment was flat within 0–5000 c/s. Due to the relatively large boundary-layer thickness and low free-stream velocity, the energy containing range of the turbulent velocity fluctuations were well below 1000 c/s. The hot-wire probes were traversed continuously in all three directions x, y and z, with an accuracy of the position co-ordinates: in $x \pm 0{\cdot}05$ cm and $y \pm 0{\cdot}01$ cm and in $z \pm 0{\cdot}10$ cm.

4.3. *The turbulence detector*

The 'turbulence detector' or 'monitor' channel consisted of a double hot-wire probe formed by two parallel wires oriented in the spanwise direction (z) separated in the normal (y) direction by a distance of $h = 0{\cdot}5$ cm. Each wire's linearized output was fed into a differential amplifier to give an output approximately proportional to the derivative,

$$u(y+h,t) - u(y,t) \approx \frac{\partial u}{\partial y} h.$$

An analogue differentiating amplifier formed the time derivative

$$S(t) = \frac{\partial^2 u}{\partial y \, \partial t}$$

required for the detector circuit (see the appendix).

The detector circuit proper consisted of another differentiator to form

$$K \frac{dS}{dt} = K\dot{S}(t).$$

By adjusting the calibrated gain K of the differentiator, the r.m.s. levels can be matched, so that

$$\overline{S^2} = K^2 \overline{\dot{S}^2},$$

and then by reading the required value of K, the characteristic time or frequency of the turbulence was determined

$$T_{ch} = f_{ch}^{-1} = 2\pi K.$$

Thus, by measuring $\overline{S^2}$ and T_{ch} in the fully turbulent region of the boundary layer,

the threshold, $C = \frac{1}{2}\sqrt{\overline{S^2}}$, and 'hold time', $\tau_H = T_{ch}/2$, were set as a first approximation. Later, more elaborate adjustments were made after the characteristics of the intermittency and turbulent structure became better known. The actual performance of the method of the detection and the actual detector circuits were extensively studied and checked by using 'synthetic signals' simulating $S(t)$. These were formed by a square wave with a variable duty factor modulating a random Gaussian noise. Details of detector and its calibration will be reported elsewhere.

The output of the detector gave $I(t-\tau_H)$, namely $I(t)$ delayed by τ_H, the 'hold time'. For the conditional sampling, $Q(t)$, the signal to be sampled was also delayed by τ_H in order to bring it 'in register' with the detector signal.

When measuring cross-correlation of $I(t)$ and another variable (u or v) no extra delay-line was used but the extra time delay τ_H was added to (or subtracted from) the time delay read on the correlator. The random square wave $I(t)$ was also fed into a pulse modulator to produce a pulse train of typically $f_p = 2\,\mathrm{kc}$ modulated by $I(t)$. By counting the pulses during a fixed time interval (typically 50 sec), γ was read directly on an electric counter.

The number of turbulent bursts per unit time, called the intermittency frequency f_γ, was measured by a frequency counter by counting the 'on' periods of $I(t)$.

4.4. *Conditional averaging*

The actual sampling and averaging was carried out by a 'Boxcar integrator'; Model CW-1, manufactured by the Princeton Applied Research Corporation of Princeton, New Jersey. In essence, the boxcar integrator is a variable-time-constant RC integrator circuit whose input is connected to $Q(t)$, the signal to be sampled, through an insulated gate field effect transistor (IGFET) acting as a high speed, extremely low leakage switch. The gate is activated when triggered by another input signal. For zone averages, $I(t)$ or $1-I(t)$ (by merely reversing polarity) was used to trigger the gate. For point averages, $\hat{P}(t)$ or $\check{P}(t)$ initiated a 'switch-on' pulse of an appropriate width to hold the gate open. The pulse trains $\hat{P}(t)$ and $\check{P}(t)$ were obtained by first differentiating $I(t)$ with respect to time, then rectifying the resulting positive and negative pulse trains. One polarity gives $\hat{P}(t)$ and the other $\check{P}(t)$.

The boxcar integrator output, i.e. the voltage across the integrating capacitor, will rise to its asymptotic value exponentially with a few time constants during which times the gate is kept open (switch closed), then it remains constant while the gate is closed (switch open). The effective averaging time depends on the pulse rate, pulse width or duty cycle, and the intrinsic time constant of the RC integrator. These are all adjustable so it was always possible to have an effective integrating time of the order of 20–50 sec. This permitted averages to be taken over a total of 1000–5000 turbulent bursts. The zone averages converge more rapidly since contributions to the total integral accumulate as fast as γT_T, where T_T is the total integration time; while point averages converge more slowly, because the contributions arrive only as one pulse per turbulent burst or as

$$f_\gamma T_p T_T,$$

where f_γ is the average frequency of the bursts and T_p is the sampling pulse width.

It must be mentioned here again that, for conditional sampling and averaging, the signal $Q(t)$ to be sampled was first delayed by a fixed delay τ_H (typically 4 msec), in order to compensate for the intrinsic delay of the turbulence detector. An analogue passive delay line was used, type 802 G, manufactured by Ad-Yu Electronics, Inc., of Passaic, New Jersey. It consists of 240 sections of passive LC networks, capable of a maximum time delay of 0–10 msec in small, microsecond increments and having a useful band width of 0–1400 c/s.

When forming the instantaneous square or product in order to conditionally sample and average fluctuation levels, a Philbrick Model MU/DV Multiplier was used. Its frequency response was 0–2 kc. Additional amplifiers were also used, which were Philbrick Model K2-W chopper stabilized amplifiers with frequency response 0–50 kc. The electronic counter used both for the determination of γ and f_γ was Model 6144 Universal EPUT and Timer manufactured by Beckman Instruments, Inc.

It may be mentioned here that similar signal processing may be performed entirely by a digital computer using multi-channel hot-wire records as suggested by Kaplan & Laufer (1969). It was felt, however, that in the present exploratory state of the research, the use of analogue methods were more flexible and cheaper, both in equipment and operating costs.

4.5. *Correlation measurements*

The correlation coefficients were determined by a Correlation Function Computer, Model 101, manufactured by Princeton Applied Research Corporation, Princeton, New Jersey. The correlator calculates the cross-correlation (or auto-correlation) simultaneously at 100 delay steps

$$R_{PQ'}(n) = \overline{P(t-[N+n]\Delta t)Q(t)},$$

where n is an integer, so that $1 \leqslant n \leqslant 100$ and $N = 0, 100, 200, 300$.

The time step Δt is adjustable within wide ranges. The output of the correlator can be recycled and observed as a periodic function on a cathode ray oscilloscope or it can be read out slowly and plotted on a standard X–Y recorder. Because of the available built-in scanning in time delay, it was a great advantage to use T, the time delay, as one of the display variables. The computional accuracy of the correlator was 3 % and the time delay accuracy was 0·5 %.

5. Experimental results

5.1. *Mean flow*

The boundary layer mean velocity profile at the $x = 900$ cm station is shown in figure 1. It was measured and plotted in the usual manner to obtain the friction velocity u_* from the 'law of the wall' as suggested by Clauser (1954). This value was checked again by measuring $\partial\overline{U}/\partial y$ in the viscous sublayer.

The boundary-layer mean flow parameters are as follows:

Free-stream velocity (nominal value at $x = 900$ cm), $U_\infty = 430$ cm/sec.
Conventional thickness ($y = \delta$, where $\overline{U} = 0{\cdot}99\ U_\infty$), $\delta = 10$ cm.
Displacement thickness, $\delta_* = 1{\cdot}56$ cm.
Momentum thickness, $\theta = 1{\cdot}08$ cm.
Shape parameter, $H \equiv \delta_*/\theta = 1{\cdot}46$.
Friction velocity, $u_*/U_\infty = 0{\cdot}045$.
Reynolds number, $U_\infty\delta/\nu = 27{,}500$.

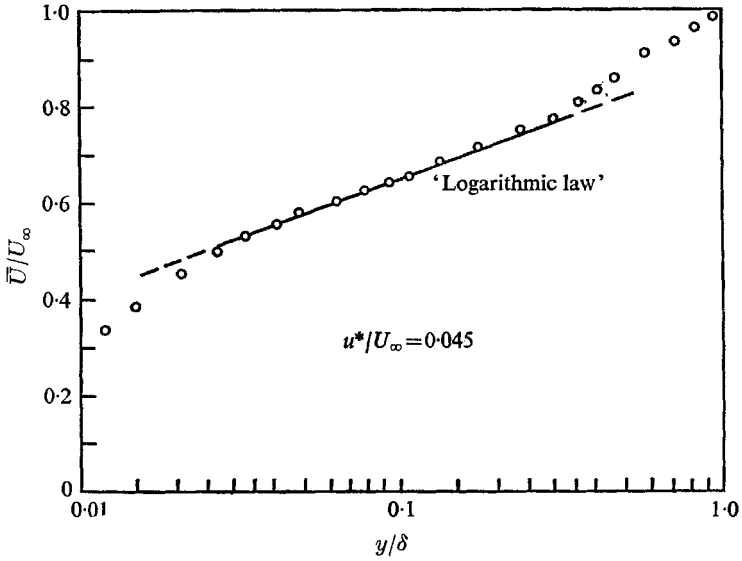

FIGURE 1. Mean velocity distribution and the determination of the friction velocity.

The mean velocity varied slightly along the test section 775 cm $< x <$ 1125 cm. There was a small positive velocity gradient, consequently the non-dimensional pressure gradient at the test station was slightly favourable

$$\frac{\theta}{\rho u_*^2}\frac{dp}{dx} = -0{\cdot}012.$$

According to Fiedler & Head (1966), in a boundary layer with a favourable pressure gradient, the intermittent zone is wider than in one with zero pressure gradient. It was felt, however, that this small departure from zero pressure gradient did not cause any significant changes in the character of the flow structure.

The free-stream turbulence level measured at $y = 2\delta$ was $u'/U_\infty = 0{\cdot}0035$, a little higher than ideal, but still acceptable, since the research was concentrated on the high intensity turbulence within the boundary layer.

5.2. *Intermittency factor and frequency*

With the customary assumption that the instantaneous position of the interface, $\eta(x, z, t)$ is a single-valued function, the function $\gamma(\eta)$ also represents the statistical

distribution of the instantaneous thickness of the turbulent region. The derivative $(d\gamma/dy)_{y=\eta}$ can be regarded as the probability density of the instantaneous interface position η. At the beginning of each day $\gamma(y)$ and δ were remeasured in order to establish the exact y positions for the desired y/δ and γ values. The $\gamma(y)$ distributions were generally repeatable on a given day after having operated the tunnel for about 1 h and the thermal conditions were stabilized in the room, but significant variations were observed from day to day. The precise

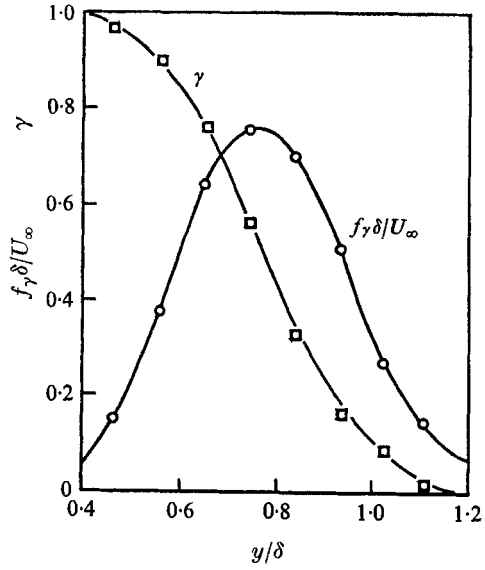

FIGURE 2. Intermittency factor γ and the intermittency frequency f_γ across the boundary layer.

form of the dependence of the intermittency distribution on temperature stratification of the laboratory was not clearly established. The nominal average position of the interface where $\gamma = 0{\cdot}5$ was found to be typically at $y = \overline{\eta} = 0{\cdot}8\delta$. It was established earlier by Corrsin & Kistler (1955) that the probability density function of the instantaneous interface position η is very nearly Gaussian, therefore $\gamma(y)$ may be approximated by the error function,

$$\gamma(y) = \frac{1}{2}\left[1 - \operatorname{erf}\left(\frac{\eta - \overline{\eta}}{\sqrt{2}\,\sigma}\right)\right]_{\eta=y}, \tag{21}$$

where

$$\operatorname{erf}\chi \equiv \frac{2}{\sqrt{\pi}}\int_0^x e^{-\xi^2} d\xi;$$

here $\overline{\eta}$ is the average position of the interface and σ is the standard deviation. For convenience it was assumed that $y = \overline{\eta}$ where $\gamma = 0{\cdot}5$. The values obtained are

$$\frac{\sigma}{\delta} = 0{\cdot}15, \quad \frac{\sigma}{\overline{\eta}} = 0{\cdot}18, \quad \frac{\overline{\eta}}{\delta} = 0{\cdot}8.$$

The intermittency frequency or interface crossing rate, $f_\gamma(y)$, is given in the non-dimensional form $(f_\gamma \delta)/U_\infty$. The maximum rate always occurs near $\gamma = 0{\cdot}5$ and f_γ decreases both for larger and for smaller intermittency values. The distributions of $\gamma(y)$ and $f_\gamma(y)$ are shown in figure 2.

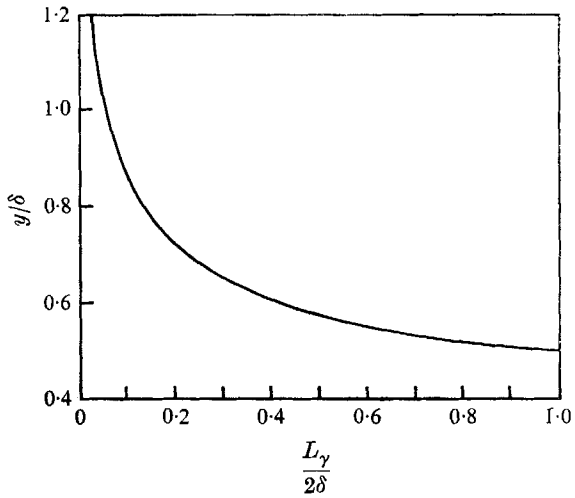

FIGURE 3. Average length L_γ of the turbulent bursts.

One may calculate the average length of the turbulent bursts from γ and f_γ. The average time between successive turbulent bursts is f_γ^{-1} and the average duration of a turbulent burst becomes γf_γ^{-1}. In order to convert the duration into a length, one must assume a numerical value for U_c, the convection velocity of the interface. Later measurements have shown that U_c is nearly equal to the free-stream velocity (see figure 16), so, by assuming here

$$U_c = U_\infty,$$

the error committed is only of the order of 5–7 %. The average length of a turbulent burst is therefore given approximately as

$$L_\gamma(y) = \frac{\gamma(y) U_\infty}{f_\gamma(y)},$$

and is shown in figure 3. One half of the length $\frac{1}{2}L_\gamma$ was plotted by assuming naively that the 'Fronts' and 'Backs' have identical shapes. The average slope of the interface was also calculated as

$$\left(\frac{dy}{dx}\right)_{\text{interface}} = 2\left(\frac{dL_\gamma}{dy}\right)^{-1}.$$

The accuracy obtainable from graphical differentiation is of course poor, but the estimated magnitude of the slope was found to be approximately

$$\left|\frac{dy}{dx}\right|_{\text{interface}} = 0{\cdot}45 \quad \text{at} \quad \gamma = 0{\cdot}5.$$

The record of the intermittency function $I(t)$ appears as a random square wave. The power spectrum of $I(t)$ measured at $\gamma = 0{\cdot}5$ is shown in figure 4. The comparison is quite favourable, with the theoretical curve representing a random square wave with transitions from 0 to 1 and from 1 to 0 occurring at instants obeying a Poisson distribution. The lack of any significant peak in the spectrum strongly discourages speculations about an instability or resonance phenomenon, such as suggested by Townsend (1966). Similar findings about the spectrum were reported earlier by Corrsin & Kistler (1955).

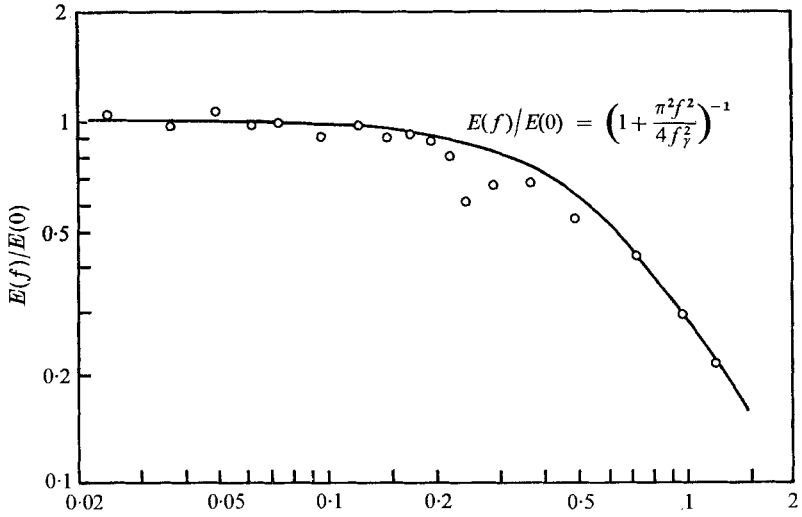

FIGURE 4. Power spectrum of the intermittency function, $I(t)$, at $\gamma = 0{\cdot}5$.

5.3. *Conditional averages of U and V*

The first application of conditional sampling was to measure the zone averages of the streamwise velocity component U both in the turbulent and in the non-turbulent zone. In figure 5 three curves are shown. First, $\overline{U}(y)$ the conventional mean velocity distribution in the boundary layer, is given (no measured points are shown). The upper curve is $\widetilde{U}(y)$, the zone average taken in the non-turbulent region, and the lower curve $\widetilde{\overline{U}}(y)$, the zone average taken in the turbulent zone. As a guide, the intermittency factor $\gamma(y)$ is also shown. The two zone averages differ by as much as 6 % and the largest difference was found in the high intermittency region where the non-turbulent fluid in the 'valleys' or 'crevices' appears to move much faster than the turbulent fluid at the same level.

The point average of the streamwise velocity component U is given in figure 6. The detector probe was placed at five different fixed positions characterized by the corresponding values of the intermittency factor

$$\gamma(y_D) = 0{\cdot}1; 0{\cdot}2; 0{\cdot}3; 0{\cdot}4; 0{\cdot}5,$$

while the signal probe was traversing in y. The resulting family of five curves $\hat{U}(y)$ each represent an (ensemble) average of the instantaneous velocity profile

across the interface with γ as a parameter. In addition, the conventionally averaged velocity $\overline{U}(y)$ is also given as a solid line (without points). The results immediately show two facts. First, the velocity did not appear to have any discontinuity at the interface. Second, the $d\hat{U}/dy$ slope that represents mean vorticity was nearly constant inside the turbulent zone and its magnitude was significantly larger than the mean vorticity $d\overline{U}/dy$. The five curves in figure 6 are in fact so similar to each other that they were replotted in such a way that the distance was measured from the location of the interface, defined as y_D, and the velocity was measured as a defect (or excess) relative to $\hat{U}(y_D)$ the velocity at the interface. The replotted data are shown in figure 7. The velocity dis-

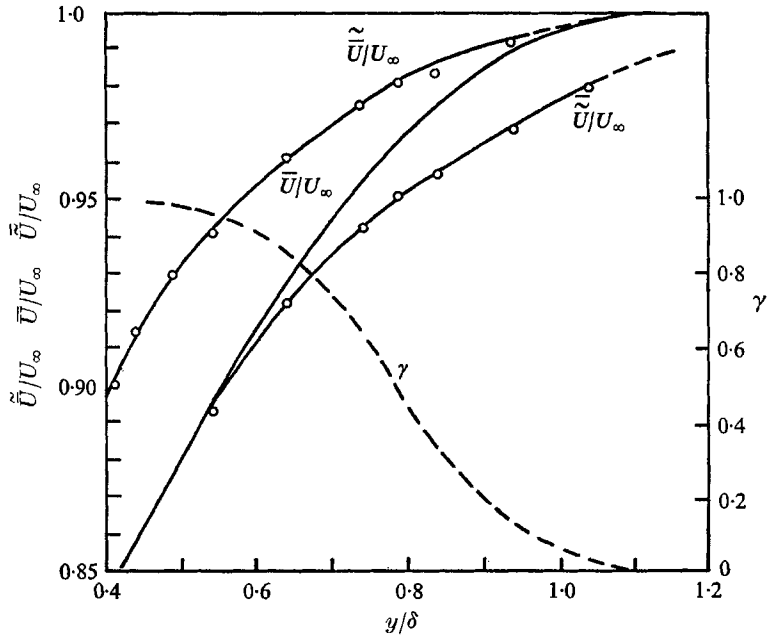

FIGURE 5. Zone averages of the streamwise velocity component. (The intermittency factor γ is given for reference.)

tribution can be well represented with a single straight line within the turbulent zone, although there was more scatter in the non-turbulent flow outside the interface. From the observed nearly constant slope, one may define the non-dimensional velocity gradient (or mean vorticity) within the turbulent fluid

$$K \equiv \frac{\delta}{u_*}\frac{d\hat{U}}{dy} \approx 8{\cdot}3.$$

A linear velocity profile near the interface was predicted by Nee & Kovasznay (1969) using a simple model based on the assumption that the effective turbulent viscosity obeys a 'rate equation.'

Since the point average of the velocity within the turbulent zone decreases proportionally to $\eta - y$, the 'depth' below the interface, almost independent

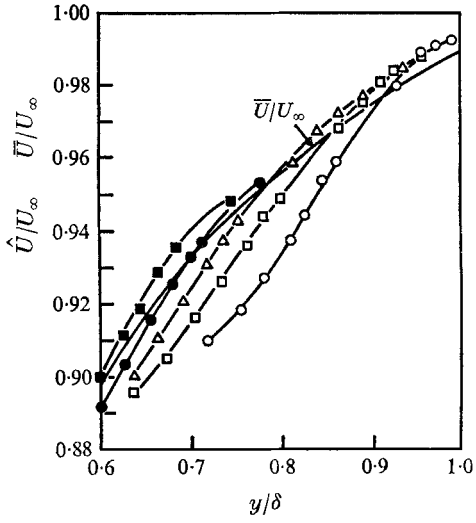

FIGURE 6. Point averages of the streamwise velocity component. The detector probe was located at the five indicated intermittency values. $\gamma(y_D)$: ○, 0·1; □, 0·2; △, 0·3; ●, 0·4; ■, 0·5.

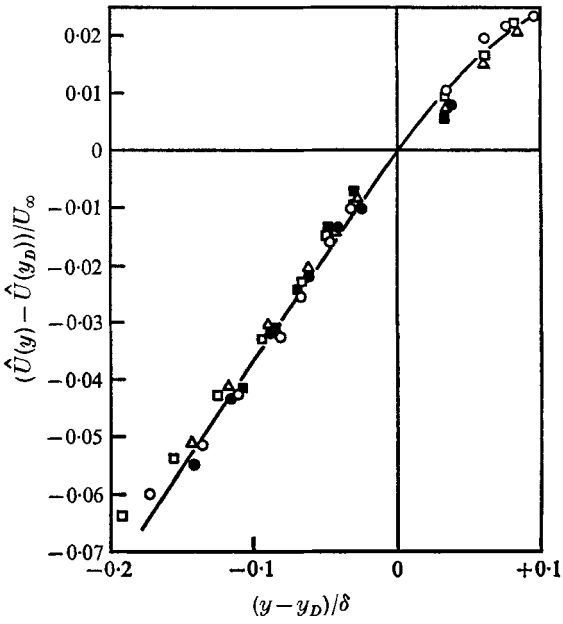

FIGURE 7. Data in figure 6 replotted as the velocity defect relative to the velocity at the interface, as a function of the distance from the interface. $\gamma(y_D)$: ○, 0·1; □, 0·2; △, 0·3; ●, 0·4; ■, 0·5.

of the instantaneous position η of the interface, the difference between zone averages (figure 5) is also understood. The difference between $\overline{\tilde{U}}$ and $\tilde{\overline{U}}$ is partly due to the 'average depth' below the interface and partly due to the velocity variation within the non-turbulent potential flow, since

$$\tilde{\overline{U}} - U_\infty \neq 0.$$

Next the conditional averages of the normal component V were measured. The mean value $\overline{V}(y)$ is quite small due to the presence of the solid wall. Calculated from the rate of the boundary-layer growth on the basis of the similarity hypothesis,

$$\overline{V}(y) < 0{\cdot}005 U_\infty$$

everywhere in the boundary layer, so it was convenient to measure and plot only the conditional average of the departure from the mean value.

The zone averages $\overline{\tilde{V}}(y)$ and $\tilde{\overline{V}}(y)$ are shown in figure 8 and the estimated $\overline{V}(y)$ is also indicated. The systematic positive value in the turbulent zones show that, in the average, the turbulent bursts move away from the wall into the potential flow. Closer to the wall, where the intermittency is high, there is an especially pronounced rapid movement toward the wall, therefore here might be a significant entrainment into the turbulent zone. The distribution of point averages of the normal velocity component V is shown in figure 9. Since the point averages at the 'Fronts' and 'Backs' were quite different, two separate families of curves are given. The abscissa is $y - y_D$, the distance from the interface, and the parameter is $\gamma(y_D)$, the intermittency factor measured at y_D. The two sets of curves reveal a rather complex picture. Since the outside flow is essentially potential, the magnitude of $\hat{V} - \overline{V}$ and $\check{V} - \overline{V}$ always decreases with increasing distance from the interface. The maximum values of $|\hat{V} - \overline{V}|$ and $|\check{V} - V|$ always occur slightly inside the turbulent zone, but the magnitude again decreases toward the wall. There is a general trend for a negative normal velocity (directed towards the wall) in the deep valleys where the interface is closest to the wall (thus corroborating the results of zone averages, shown in figure 8) and a small positive value (away from the wall) is seen deep in the turbulent region, especially when the interface is in an extreme position (e.g. the small positive values shown on the curve 'Front' $\gamma = 0{\cdot}1$). It is especially interesting to note that the 'Front' and 'Back' are so different. At the 'Fronts' the disturbances are essentially negative for all positions of the interface, but, at the 'Backs', $\hat{V} - \overline{V}$ is positive for $\gamma(y_D) < 0{\cdot}6$ and negative for $\gamma(y_D) > 0{\cdot}6$. This is tentatively suggestive of a stagnation point on the 'Back' around $\gamma = 0{\cdot}6$, $(y/\delta = 0{\cdot}7)$ if the phenomenon is viewed from a co-ordinate system moving with the average convection velocity of the interface.

5.4. *Conditionally averaged fluctuation levels*

As was indicated earlier, conditional averages of the mean square fluctuations can be obtained by sampling the instantaneous square of a fluctuating quantity whose conditional average is made zero by subtracting the corresponding mean value. Then, by taking the square root of such a conditional mean square

value, a conditionally averaged fluctuation level can be defined. First, the instantaneous fluctuation around a conditional average value will be defined. Let

$$u_1(t) = U(t) - \tilde{\bar{U}} \quad \text{and} \quad u_2(t) = U(t) - \tilde{\bar{U}},$$

so that

$$\tilde{\bar{u}}_1 = \tilde{\bar{u}}_2 = 0, \quad \text{then} \quad \tilde{\bar{u}}' \equiv \sqrt{\tilde{\bar{u}}_1^2} \quad \text{and} \quad \tilde{\bar{u}}' \equiv \sqrt{\tilde{\bar{u}}_2^2}.$$

For completeness the conventional r.m.s. value is defined as $u' \equiv \sqrt{\overline{u}^2}$ with $u(t) = U(t) - \overline{U}$. In figure 10 three curves are given: $\tilde{\bar{u}}'$ for the turbulent zone, $\tilde{\bar{u}}'$ for the non-turbulent zone, and, for reference, u', the conventional turbulent

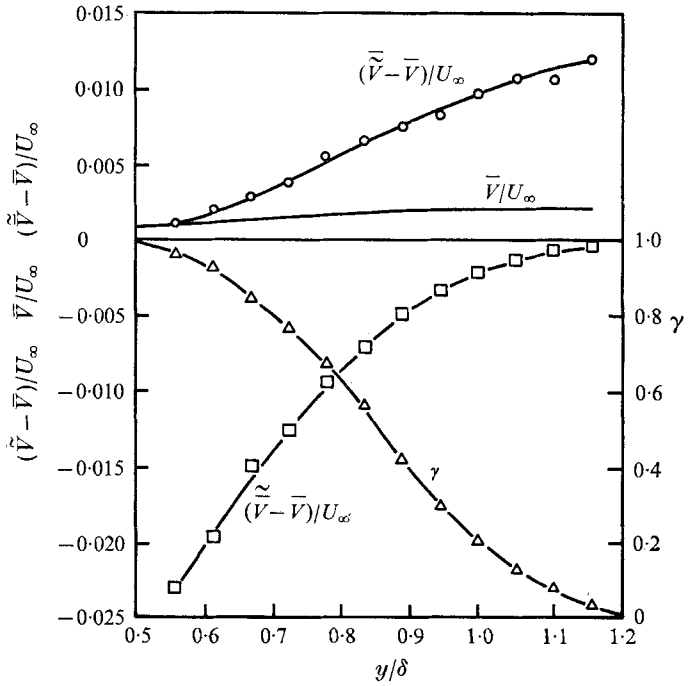

FIGURE 8. Zone averages of the normal velocity component.

intensity. Furthermore, $\gamma(y)$ is also indicated to guide the reader. The fluctuation intensity reaches a minimum level of 3 % inside the turbulent bursts far out in the low intermittency region. In the non-turbulent region, the fluctuation level increases deeper in the boundary layer; it attains a maximum near 3 % where $\gamma = 0{\cdot}9$ where the fluctuation intensity in the adjacent turbulent bursts is about double. It is clear that the usual practice of estimating the turbulent intensity within the turbulent bursts by merely dividing the mean square fluctuation intensity by the intermittency factor γ would be inappropriate here as the non-turbulent fluctuations contribute a non-negligible amount to the total fluctuation level.

The relation between the three averages is

$$(u')^2 = \gamma(\tilde{\bar{u}}')^2 + (1-\gamma)(\tilde{\bar{u}}')^2. \tag{22}$$

The data presented in figure 10 is given as r.m.s. levels and not as mean square values so $\tilde{\bar{u}}'$ and $\tilde{\bar{u}}'$ is not bisected by the half intermittency point, where $\gamma = 0{\cdot}5$.

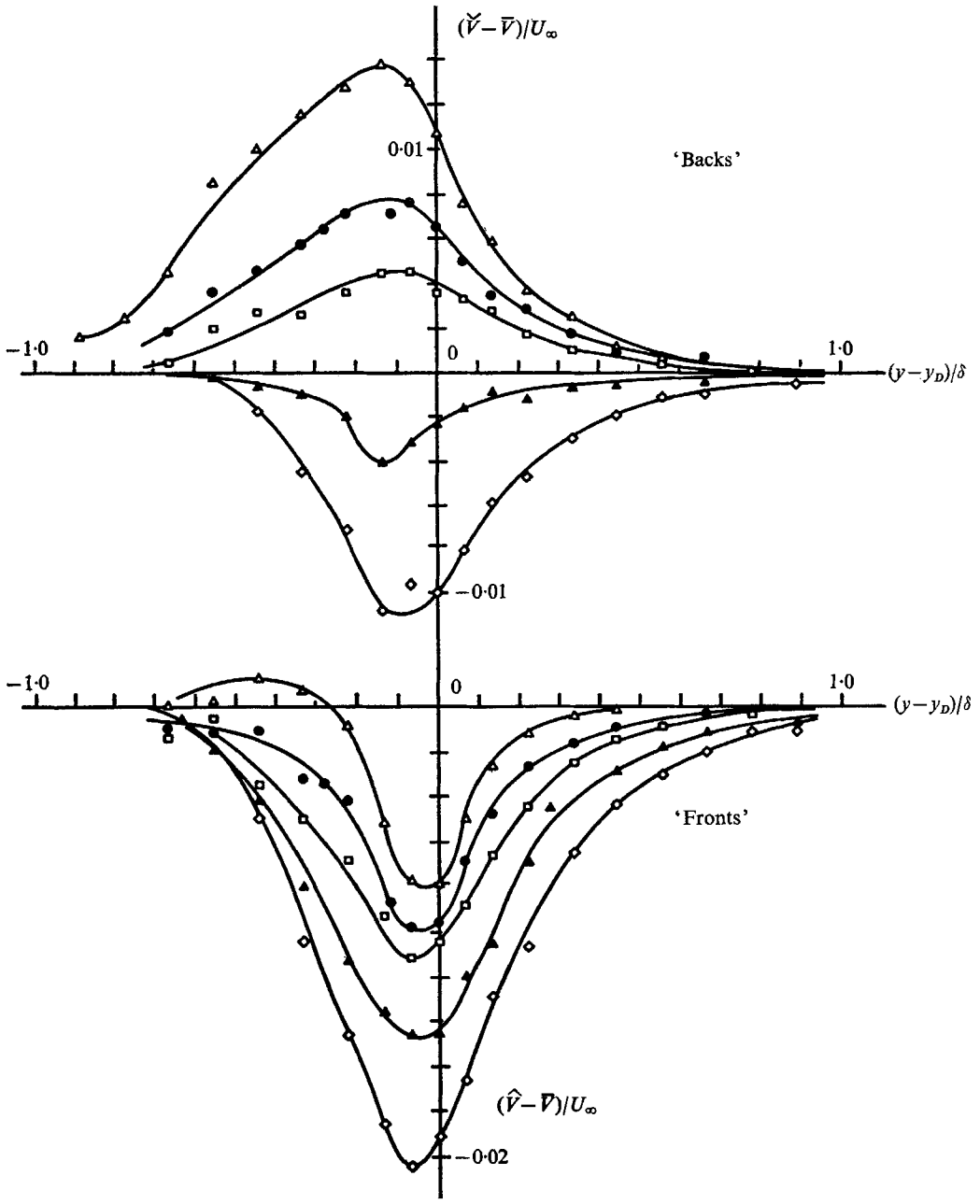

FIGURE 9. Point averages of the normal velocity component as a function of the distance from the interface. $\gamma(y_D)$: △, 0·1; ●, 0·3; □, 0·5; ▲, 0·7; ◇, 0·9.

The fluctuation intensities in the outside potential flow ($\gamma \approx 0$) far from the randomly oscillating interface have been measured for the turbulent wake by Townsend (1949), for the two-dimensional jet in a slow-moving stream by Bradbury (1965), and for the turbulent boundary layer by Klebanoff (1954) and Bradshaw (1967). All were in substantial agreement with the theory of Phillips (1955), in the sense that the fluctuation energy would vary as $(y-y_s)^{-4}$ for the distances large compared to the dimensions of the energy-carrying eddies.

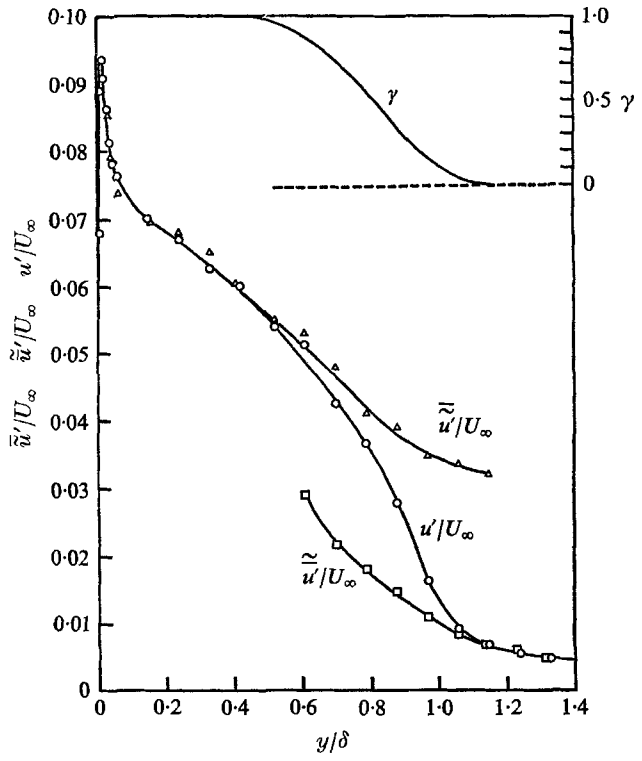

FIGURE 10. Zone average intensities of the streamwise velocity fluctuations.

The effective position of the sources, for the outside potential flow, are located inside the boundary layer at y_s that is also determined from the data. In order to check Phillips's theory, measured values of $\tilde{\tilde{u}}'$, shown in figure 10, have been replotted in figure 11. That quantity,

$$\left[\frac{(\tilde{\tilde{u}}')^2}{U_\infty^2}\right]^{-\frac{1}{4}},$$

is plotted as a function of y/δ. The linearity is surprisingly good even within the intermittent zone at least down to an intermittency level $\gamma = 0{\cdot}8$. The departure from linearity at large distances was due to the relatively high free-stream turbulence levels. The extrapolated zero-intercept gives the value,

$$y_s/\delta = 0{\cdot}25.$$

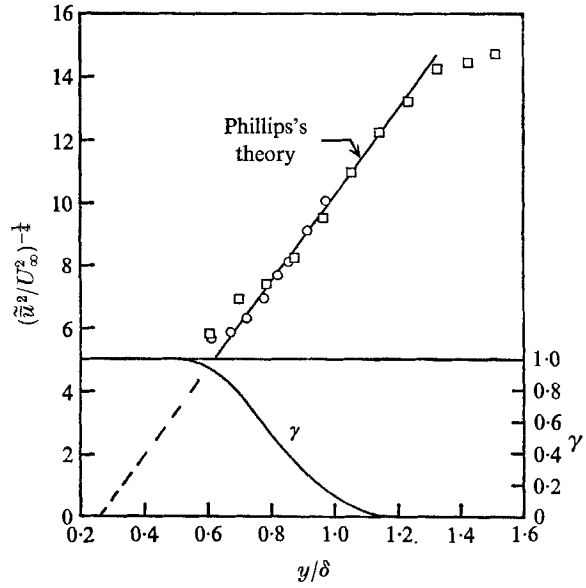

FIGURE 11. Zone averaged intensities replotted to compare with Phillips's (1955) theory.

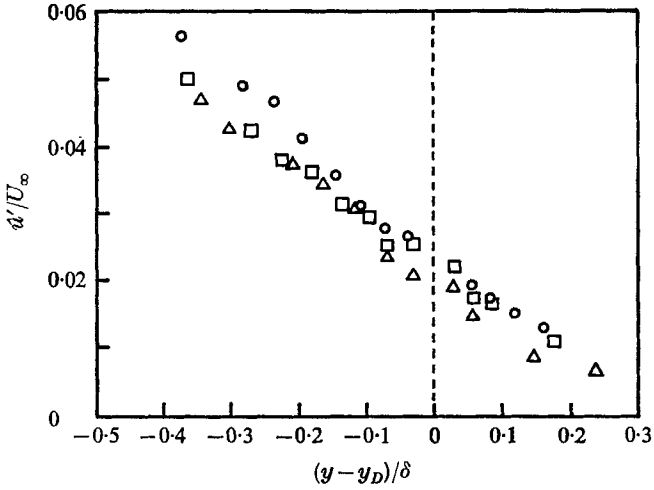

FIGURE 12. Distribution of the point averaged intensities of the streamwise velocity fluctuations across the interface. $\gamma(y_D)$: △, 0·1; □, 0·3; ○, 0·5.

Point averages of the streamwise velocity fluctuation intensities are presented in figure 12. Three curves are given, one for each detector position (where $\gamma = 0{\cdot}1, 0{\cdot}3, 0{\cdot}5$). It appears that $\hat{u}'(y)$ varies rather smoothly across the interface, consequently turbulence detectors should not be based on the velocity fluctuation intensity.

Following the work of Corrsin & Kistler (1955), it was believed that the clear distinction between the turbulent and non-turbulent regimes must be based

preferably on the vorticity fluctuation level. It is possible to measure the instantaneous streamwise component of the vorticity, as shown by Kistler (1952) and Kovasznay (1954), but only by using a special array of four matched hot-wires. In a boundary layer the mean vorticity has only a spanwise component $\Omega_z = \partial\overline{U}/\partial y$ but the fluctuating vorticity has all three components. It was felt that the instantaneous velocity gradient $\partial u/\partial y$ represents a large portion of the

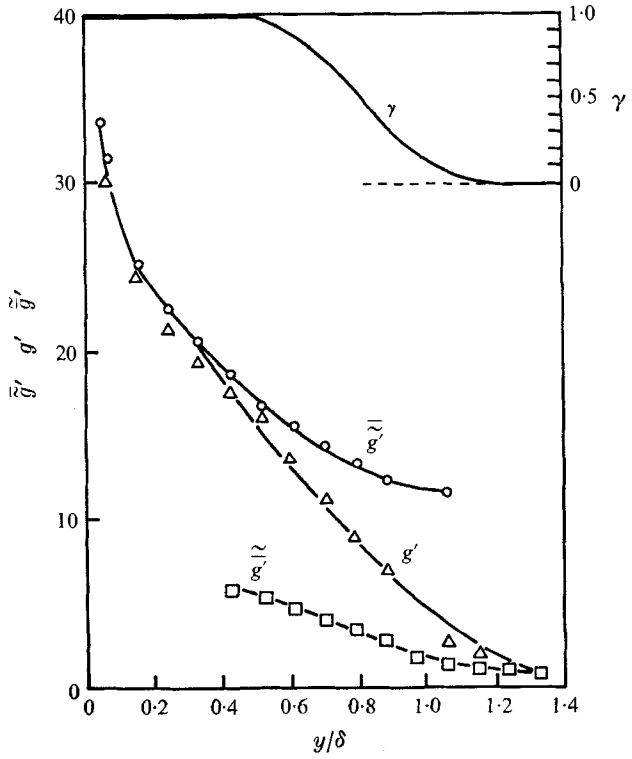

FIGURE 13. Zone averaged intensities of the velocity gradient fluctuations.

spanwise vorticity fluctuation since the contribution from the other term $\partial v/\partial x$ is expected to be smaller. One may regard here the velocity gradient $\partial u/\partial y$ as a 'quasi-vorticity'. The measurements are presented in the non-dimensional form,

$$G \equiv \frac{\delta}{u_*}\frac{u(y+h)-u(y)}{h} \approx \frac{\delta}{u_*}\frac{\partial u}{\partial y}.$$

Separating G into mean and fluctuating quantities $G(t) = G+g(t)$, so that $\bar{g} = 0$, the r.m.s. conditional averages of g were determined. The distance h of the two parallel wires was chosen to be of the order of λ_y, the lateral microscale of the turbulence. On one hand, a smaller separation would reduce the signal level (and signal-to-noise ratio); on the other hand, a larger separation would give a poor approximation to spatial differentiation, so the above compromise was made. Fortunately, the choice was found not to be too critical. Conditional averages of the mean vorticity were actually measured but not shown here

because they are equivalent to the conditional averages of U differentiated with respect to y.

Zone average fluctuation intensities of $\tilde{\bar{g}}'$ and $\tilde{\tilde{g}}'$ are shown in figure 13. The general character of the three curves is similar to that in figure 10 except for one fact, namely the ratio of the intensities in the turbulent and in the non-turbulent zones is larger here, therefore it is better to use g than u for the detection of turbulence.

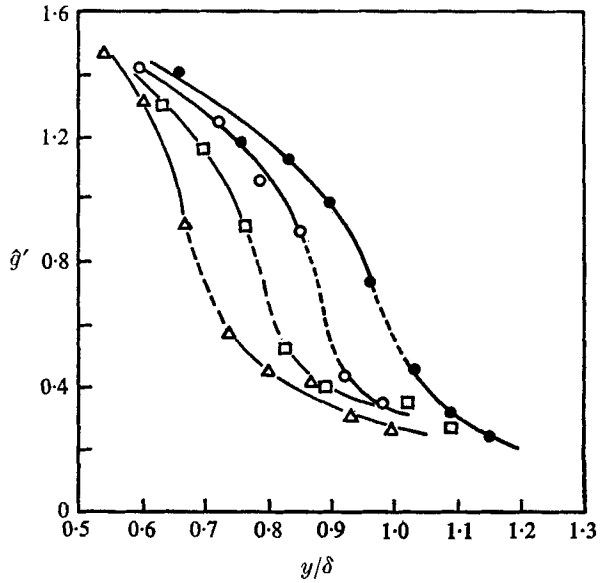

FIGURE 14. Point averaged intensities of the velocity gradient for four positions of the interface detector. Interface region is indicated by the dotted line. $\gamma(y_D)$: ●, 0·1; ○, 0·3; □, 0·5; △, 0·7.

Point averages of the velocity gradient fluctuation are shown in figure 14. The rapid increase inside the interface suggests a jump in the vorticity fluctuation level. Of course, even if the vorticity fluctuations jumped discontinuously at the interface, the velocity gradient fluctuation still would be smoother because, even in the irrotational potential flow, there are some $\partial u/\partial y = \partial v/\partial x$ fluctuations present.

In order to see that the behaviour of the quantity on which the actual interface detection is based, $S(t)$ was conditionally averaged, and the ratio of the zone averaged fluctuation levels is presented in figure 15. It is clear that the detection is better in the outer region where the intermittency is low, but even at high intermittencies there is a signal-to-noise ratio of about 10 dB. On the basis of figure 15, an improved setting of the trigger level of the detector can be made for each y_D position.

5.5. *Convection velocity of the interface*

Based on measurements outside the boundary layer, it was suggested earlier by Liepmann (1954) and later by Bradshaw (1967) that the fluctuations in the outer flow can be regarded as those of a potential flow over a random wavy wall. The

fluctuation amplitudes can be calculated or at least estimated if the relative velocity and the r.m.s. slope of the fictitious wavy wall are known. It is of course still open to question whether or not the interface itself should be regarded as the wavy wall. By using sufficient numbers of hot-wire probes, one can determine at least in principle the instantaneous fluctuation of the local displacement thickness,

$$\delta_*(x,z,t) = \int_0^\infty \left[1 - \frac{U(x,y,z,t)}{U_\infty}\right] dy,$$

but this was not attempted. Since the intermittency function $I(t)$ was available, the measurements of the convection velocity of the interface was relatively easy.

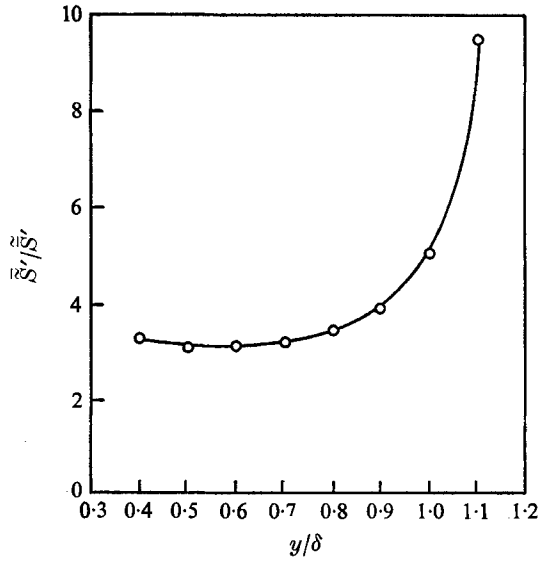

FIGURE 15. Distribution of the 'signal-to-noise' ratio of the function $S(t)$ across the boundary layer.

The space-time correlation of the intermittency function $I(t)$ does yield a convection velocity, but the local maxima of the correlation curves are not sharply defined, so that one can only state that

$$0{\cdot}9U_\infty < U_c < U_\infty.$$

A more accurate method was adopted here; namely, the space-time auto-correlation of the pulse trains $\hat{p}(t)$ and $\check{p}(t)$ (defined by (7) and (8)) was measured separately over large space separations $x - x_0 \approx 3\delta$ and the accurate values for the 'time of flight' were obtained.

Figure 16 shows the convection velocities separately for the 'Fronts' and for the 'Backs' as functions of y/δ. For reference, the mean velocity $\overline{U}(y)/U_\infty$ and the distribution of $\gamma(y)$ at the downstream station are also given. It is interesting to note that the maximum difference in convection velocities between 'Fronts' and 'Backs' was found to be near $\gamma = 0{\cdot}5$, and that they tend to become nearly

identical as $\gamma \to 1$. If the turbulent bursts have an upward thrust away from the wall as suggested by the zone average of V in figure 8, then, to a fixed observer moving downstream at a constant y, the length of the turbulent bursts would increase. A positive normal velocity in the turbulent zone $\overline{\tilde{V}}/U_\infty$ of the order of 1 % is sufficient to explain the observed difference. The measurements were taken by placing the two probes at the same value of y so the downstream station is at a slightly smaller y/δ due to the boundary-layer growth and has also a slightly larger γ. On the other hand, for $\gamma \to 0$ the top of a turbulent burst that was very short and barely detectable by the upstream probe, would give a 'Front' and 'Back' pulse with only very little time difference. But the same burst will have a longer duration when detected at the downstream station so its 'Back' will arrive later than its 'Front' and the two convection velocities remain different. The overall average value for the convection velocity is of the order of $U_c \approx 0{\cdot}93U_\infty$.

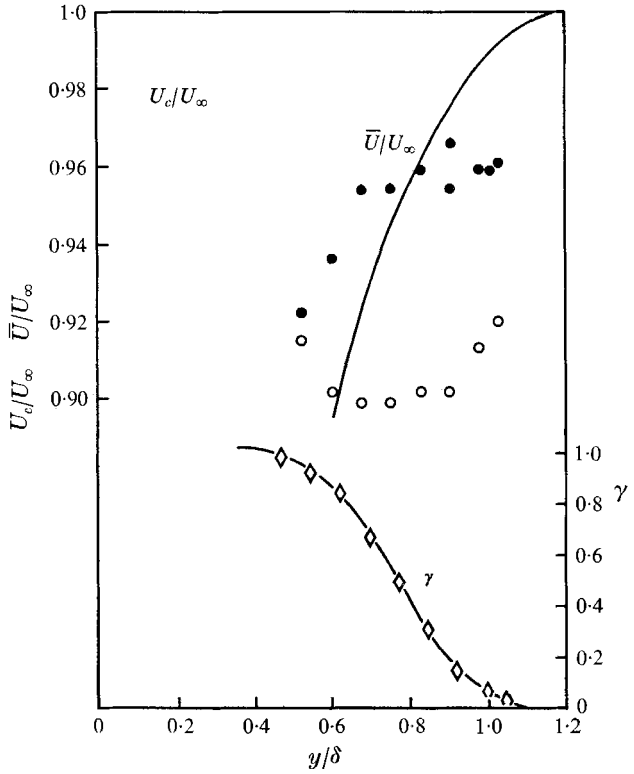

FIGURE 16. Local convection velocities of the interface. ●, fronts; ○, backs. The conventional mean velocity profile and the intermittency factor are given for reference.

5.6. *Correlation maps*

Since the correlator gave the cross-correlation of the two inputs as a function of the relative time delay at a hundred points, it was a great economy to choose T as one of the display variables and keep $X = X_0 = \text{constant}$. The correlation $R_{PQ'}(X, Y, Z, T)$ is presented with y_0/δ_0 specified separately in order to avoid

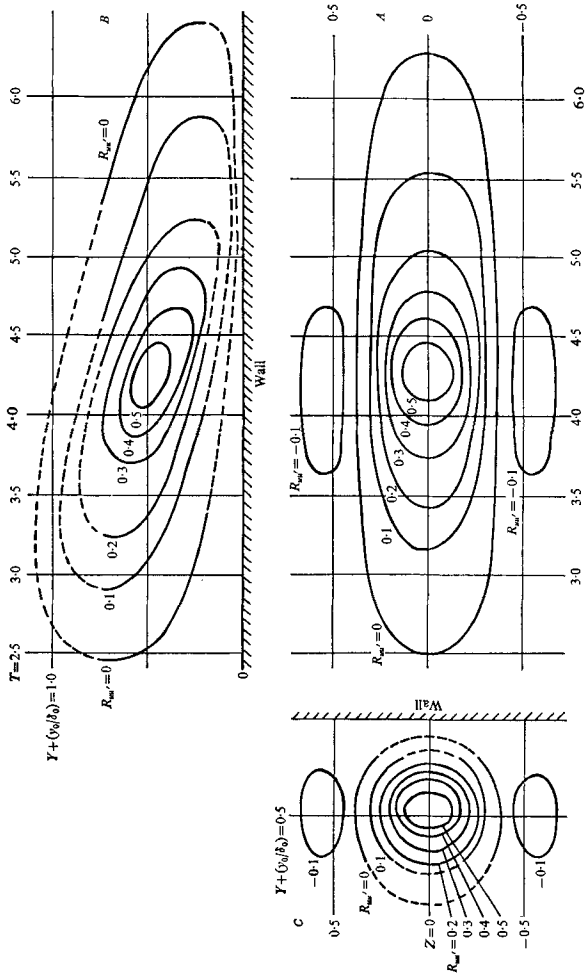

FIGURE 17. Three-dimensional representation of the space-time auto-correlation of the streamwise velocity fluctuation inside the fully turbulent region, $R_{uu'}(X_0, Y, Z, T)$ at $X_0 = 3{\cdot}8$ and $y_0/\delta_0 = 0{\cdot}5$. Section A: $Y = 0$ plane. Section B: $Z = 0$ plane. Section C: $T = 4{\cdot}27$ plane.

confusion. The majority of the maps are displayed on the Z, T plane with $X = X_0 =$ constant and $Y = 0$, although there are a few maps in the Y, T or X, Z plane. If the fixed separation distance X_0 is large, i.e. if it amounts to several boundary-layer thicknesses, then the iso-correlation surfaces reveal the average large eddy structure. Figure 17 shows the auto-correlation surfaces in three dimensions in Y, Z, T space of

$$R_{uu'}(X_0, Y, Z, T) \quad \text{with} \quad X_0 = 3{\cdot}8 \quad \text{and} \quad y_0/\delta_0 = 0{\cdot}5.$$

In this and all subsequence figures, the solid lines represent the measured values and the dashed contours are the extrapolated values.

The striking feature is the streamwise elongation of the iso-correlation surfaces. The spanwise (Z) extent of the correlation is much smaller and, in addition, two clearly negative regions are flanking the large positive body. In the normal (Y) direction, the correlation extends almost across the entire boundary layer. In the Y, Z plane, the positive iso-correlation contours appear almost circular in shape and the cross-section of the two negative correlation regions is also clearly visible. There is a moderate tilt in the Y, T plane suggestive of a similar (but mirrorwise) tilt in the X, Y plane that would be observed for $T = T_0 =$ constant and X variable.

Most of the subsequent measurements were taken with a somewhat smaller downstream separation, $X_0 = 2{\cdot}25$, because it gave higher maximum correlation values, therefore, better resolution; however, it was considered still far enough to discern the large eddy structure. In general, the separation X_0 was considered sufficient if $R_{PQ'}(X_0, Y, Z, T) \to 0$ for $T \to 0$.

Figure 18 shows $R_{uu'}(X_0, O, Z, T)$ in the T, Z plane for $X_0 = 2{\cdot}25$. The general character is the same as it is shown for the larger separation in figure 17. In the subsequent maps $X_0 = 2{\cdot}25$ was used; $y_0/\delta_0 = 0{\cdot}45$ was chosen in the fully turbulent flow and $y_0/\delta_0 = 0{\cdot}8$ ($\gamma = 0{\cdot}5$) in the intermittent zone. All exceptions will be emphasized. One of the important novel features of the present series of measurements was the exploration of the space-time auto- and cross-correlations involving v, the normal component of the turbulent velocity function.

The space-time auto-correlations of the normal component are in general more difficult to measure since they involve two pairs of hot-wires and additional care must be taken to avoid probe interference (the wake of the upsteam probe for $Y = Z = 0$). Figure 19 shows that, surprisingly enough, $R_{vv'}(X_0, O, Z, T)$ is quite different from $R_{uu'}(X_0, O, Y, T)$. First, the $R_{vv'} = 0$ contour is a closed oval line and the negative correlation outside it must be extensive but weak; it never reaches 0·05, where a contour line would have been drawn. The iso-correlation contours are all elongated in the streamwise (T) direction and the total spatial extent of the significant correlation values is smaller than for $R_{uu'}$.

The cross-correlation $R_{uv'}$, that for zero separation is proportional to the tangential Reynolds stress, is presented in two maps; $R_{uv'}(X_0, O, Z, T)$ in figure 20 and $R_{vu'}(X_0, O, Z, T)$ in figure 21. They are very asymmetrical with respect to the 'streamwise' co-ordinate (T). The lack of symmetry suggests that the rate of development of the u and v components is slightly different during their passage over the distance $2{\cdot}25\delta$. It will be seen later that this asymmetry increases in the

intermittent zone. The variation of the cross-correlation $R_{vu'}(0, 0, 0, T)$ in the outer portion of the boundary layer ($y_0/\delta_0 = 0{\cdot}6$, $0{\cdot}8$, $1{\cdot}0$ and $1{\cdot}2$) is shown in figure 22. Inside the turbulent region the $R_{vu'}$ correlation attains its largest negative values $R_{vu'} = -0{\cdot}45$ at $T = 0$ and its variation with T is roughly symmetrical

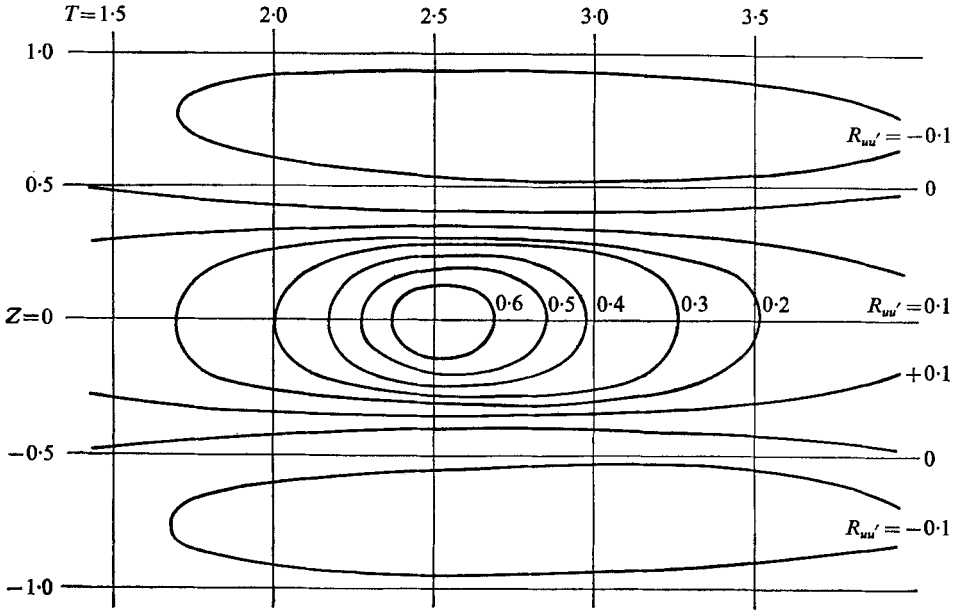

FIGURE 18. Space-time auto-correlation map of u in the fully turbulent region $R_{uu'}(X_0, O, Z, T)$ at $X_0 = 2{\cdot}25$ and $y_0/\delta_0 = 0{\cdot}45$.

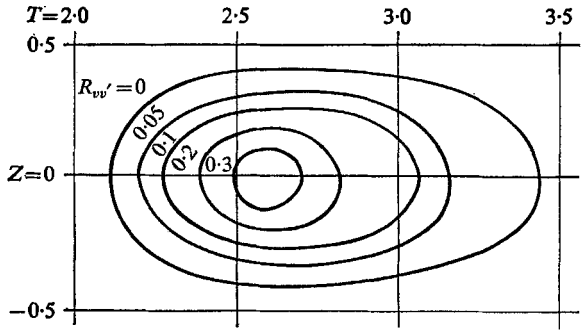

FIGURE 19. Space-time auto-correlation map of v in the fully turbulent region $R_{vv'}(X_0, O, Z, T)$ at $X_0 = 2{\cdot}25$ and $y_0/\delta_0 = 0{\cdot}45$.

(i.e. an even function of T). These results can be compared with those of Tritton (1967), who measured space correlation only; but with Taylor's hypothesis a modest comparison can be made. Outside the boundary layer, the flow is essentially irrotational and it can be approximated with a flow over a 'wavy wall'; consequently the Fourier components of u and v must be out of phase by exactly 90°. The correlation coefficient then is an odd function of the time delay T.

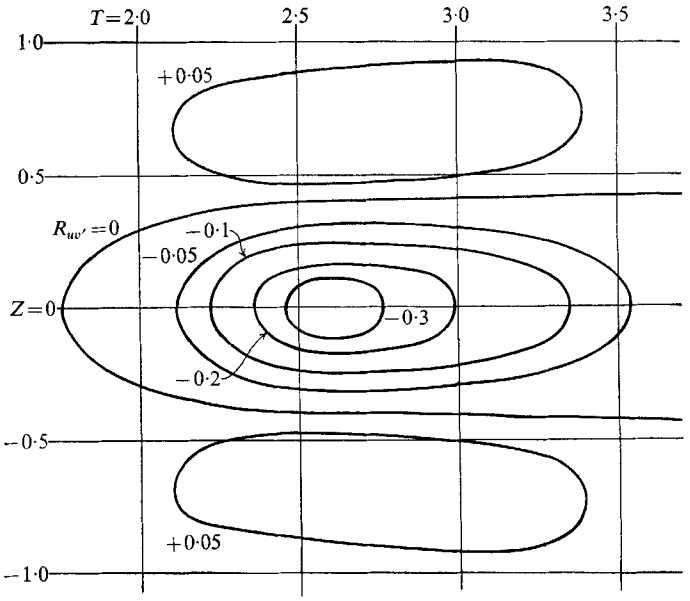

FIGURE 20. Space-time cross-correlation map in the fully turbulent region of $R_{uv'}(X_0,O,Z,T)$ at $X_0 = 2{\cdot}25$ and $y_0/\delta_0 = 0{\cdot}45$. ($u$ delayed and v taken at the downstream station.)

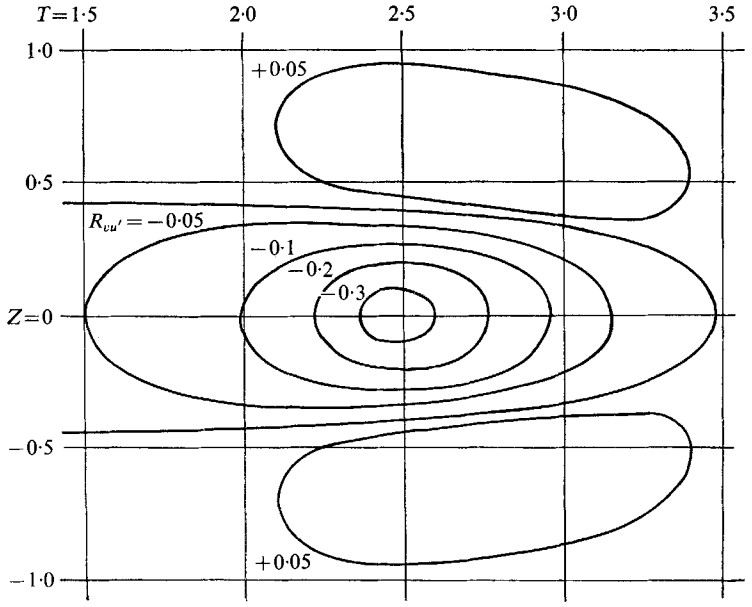

FIGURE 21. Space-time cross-correlation map in the fully turbulent region of $R_{vu'}(X_0,O,Z,T)$ at $X_0 = 2{\cdot}25$ and $y_0/\delta_0 = 0{\cdot}45$. ($v$ delayed and u taken at the downstream station.)

It is easy to see that $R_{vu'}(O, O, O, T)$ in the potential flow must be proportional to the sine Fourier transform of the power spectrum,

$$R_{vu'}(O, O, O, T) = \text{constant} \times \int_0^\infty E(f) \sin 2\pi f T \, df, \tag{23}$$

where $E(f)$ is the power spectrum of both u and v. In the intermittent zone, the correlation must be therefore a mixture of the even and odd functions of T with the proportion changing with γ.

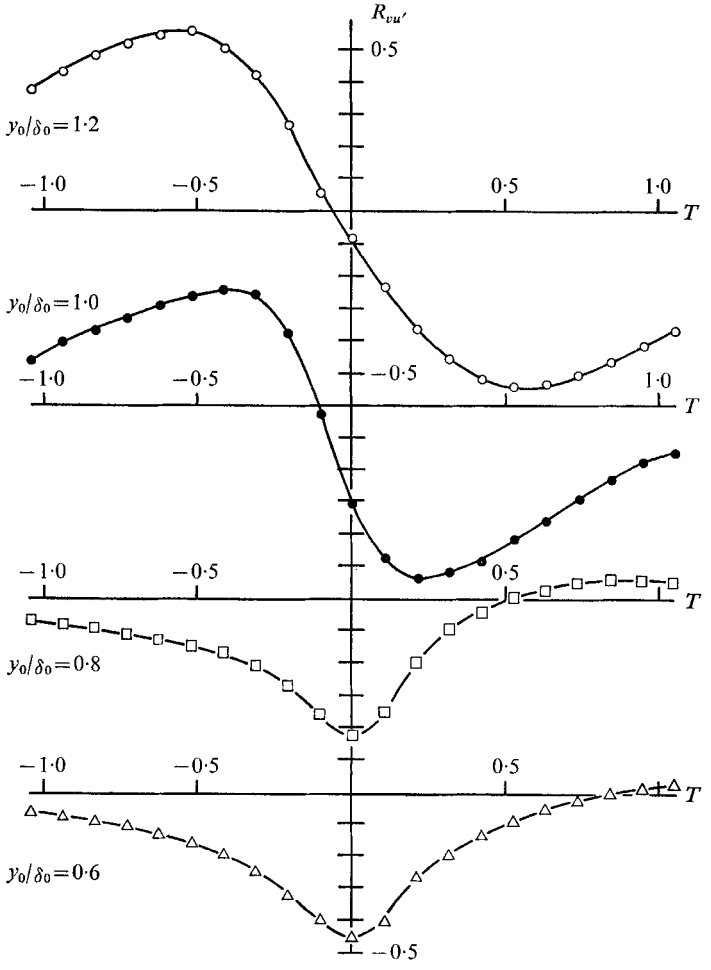

FIGURE 22. Cross-correlation of u and v at four different levels in the boundary layer $R_{vu'}(O, O, O, T)$ at $y_0/\delta_0 = 0{\cdot}6$, $0{\cdot}8$, $1{\cdot}0$ and $1{\cdot}2$.

Let us turn now to the correlation maps obtained in the intermittent region. The intermittency function $I(t)$ has non-zero mean value, consequently, (20) must be observed. The spatial auto-correlation map (with no time delay) $R_{II'}(X, O, Z, O)$ at the half intermittency level $y_0/\delta_0 = 0{\cdot}8$ and $\gamma = 0{\cdot}5$ is shown in figure 23. The contours are oval and elongated in the streamwise direction and

there are only diffuse and quite small negative correlation values. Imaki (1968) built turbulence detectors with the help of one of the authors (L. S. G. K), and has observed some negative correlations for spanwise (Z) separation in his boundary layer. The source of this discrepancy has not been resolved yet. The space-time auto-correlation of the intermittency function $R_{II'}(X_0, O, Z, T)$,

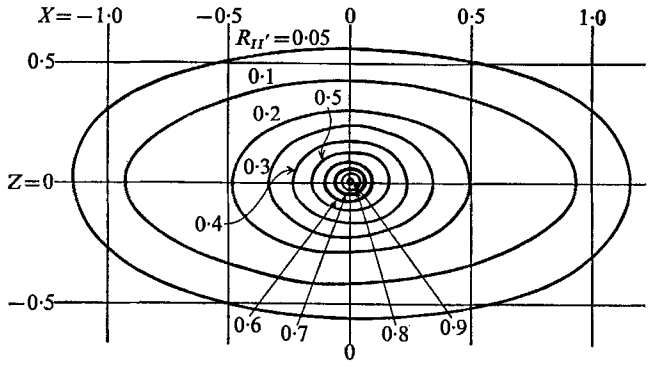

FIGURE 23. Spatial auto-correlation map of the intermittency function $R_{II'}(X, O, Z, T)$ at half intermittency level, $y_0/\delta_0 = 0{\cdot}8$.

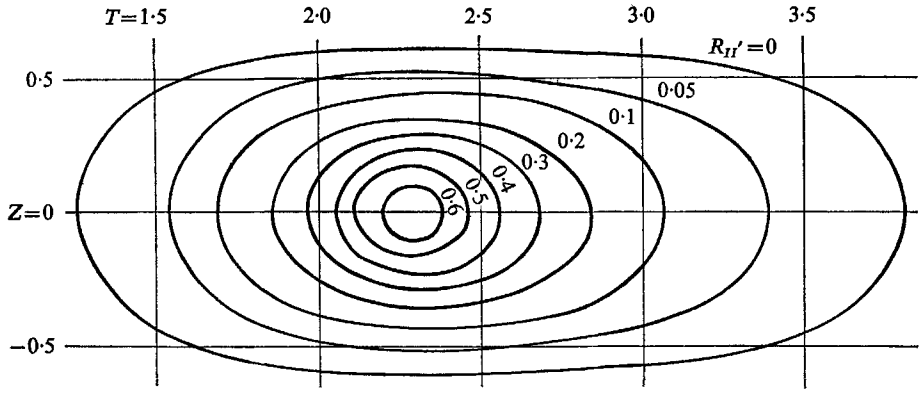

FIGURE 24. Space-time auto-correlation map of the intermittency function $R_{II'}(X_0, O, Z, T)$ at the half intermittency level at $X_0 = 2{\cdot}25$ and $y_0/\delta_0 = 0{\cdot}8$.

with $X_0 = 2{\cdot}25$ at the half-intermittency level, is given in figure 24. The iso-correlation contours are oval and elongated in the streamwise direction with an aspect ratio of nearly 2:1. The zero-correlation contour is also an oval, indicating small negative values in the outside. The maximum correlation coefficient is quite high, $R_{II'\max} = 0{\cdot}65$, indicating a good persistency of the intermittency pattern during its travel downstream, a distance of $2{\cdot}25\ \delta_0$.

The space-time auto-correlation of the streamwise velocity $R_{uu'}(X_0, O, Z, T)$ with $X_0 = 2{\cdot}25$, $y_0/\delta_0 = 0{\cdot}8$ and $\gamma = 0{\cdot}5$ is given in figure 25. It is quite similar to the one measured deeper in the fully turbulent region boundary layer shown in figure 18. The pattern is somewhat less elongated than the one with $X = 2{\cdot}25$ deeper in the layer.

The space-time auto-correlation of the normal component $R_{vv'}(O, O, Z, T)$ is given in figure 26 and $R_{vv'}(X_0, O, Y, T)$ with $X_0 = 2{\cdot}25$ is given in figure 27. The iso-correlation contours of figure 26 are nearly circular and only small negative values are present outside the $R_{vv'} = 0$ circle. The appearance of figure 27 is different. Not only is the spanwise (Z) spread of the correlation somewhat more extended than in figure 26, but also distinct negative values appear in the fore and aft streamwise (T) directions. This point will be discussed later. The space-time auto-correlation of the normal component in the normal plane $R_{vv'}(X_0, Y, O, T)$ is shown in figure 28. The upstream probe is fixed at $y_0/\delta_0 = 0{\cdot}78$ and the downstream wire is at $X_0 = 2{\cdot}25$. The iso-correlation contours are plotted in the Y, T plane. It is interesting to note that the $R_{vv'}$ auto-correlation persists far outside the boundary layer into the potential region as far as $y = 2\delta$.

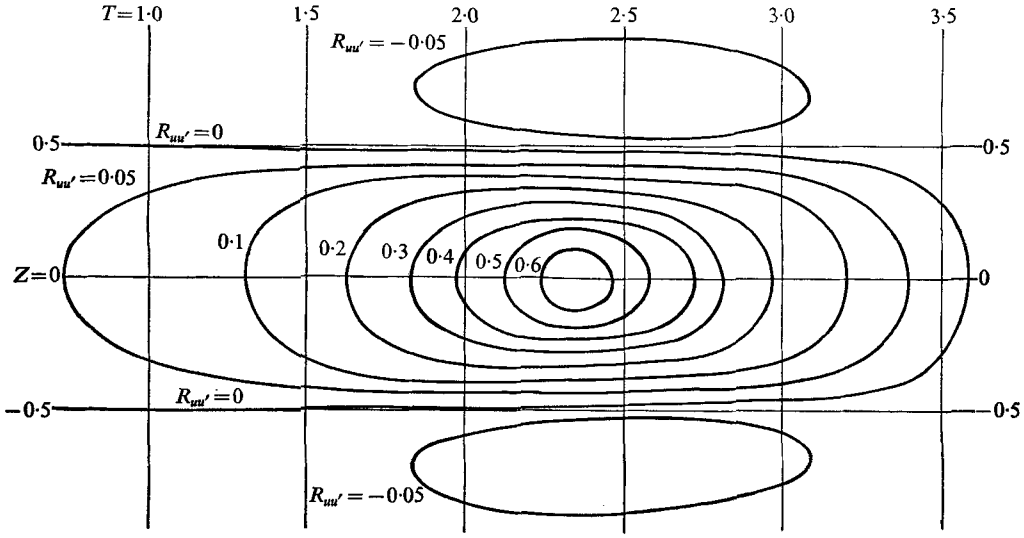

FIGURE 25. Space-time auto-correlation map of u at the half intermittency level $R_{uu'}(X_0, O, Z, T)$ at $X_0 = 2{\cdot}25$ and $y_0/\delta_0 = 0{\cdot}8$.

Space-time cross-correlations involving the intermittency function were also measured. The map for $R_{uI'}(X_0, O, Z, T)$ with $X_0 = 2{\cdot}25$ and $y_0/\delta_0 = 0{\cdot}8$ is shown in figure 29. The correlation is mostly negative, indicating that the streamwise velocity in the turbulent bursts is generally less than the local average velocity. This is of course consistent with the conditional zone averages shown in figure 5. It is important to note that the pattern is also a nearly symmetrical oval shape quite similar to $R_{II'}$ itself, thus strongly suggesting a nearly one-to-one correspondence between I and u, at least as far as the large scale is concerned. However, the distinct negative lobes of $R_{uu'}$ in the spanwise direction do not appear in $R_{uI'}$.

The space-time cross-correlation of u and v $R_{vu'}(X_0, O, Z, T)$ and $R_{uv'}(X_0, O, Z, T)$ with $X_0 = 2{\cdot}25$ at the half intermittency level, $\gamma = 0{\cdot}5$, were measured and are given in figures 30 and 31. The fact that the two maps are

different shows that the u and v components have developed differently during their journey downstream.

It is interesting to compare figure 30 and 31 with the map of the same correlation but without separation in the streamwise co-ordinates. Figure 32 shows $R_{vu'}(O, O, Z, T)$ also at $\gamma = 0{\cdot}5$. The $Z = 0$ cut is almost identical with the curve given in figure 22 for $y_0/\delta_0 = 0{\cdot}8$. The contribution from the small-scale eddies

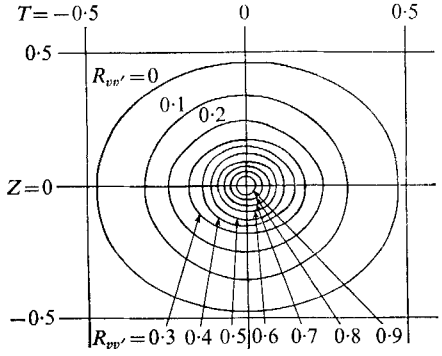

FIGURE 26. Space-time auto-correlation map of v at the half intermittency level $R_{vv'}(O, O, Z, T)$ with $y_0/\delta_0 = 0{\cdot}8$.

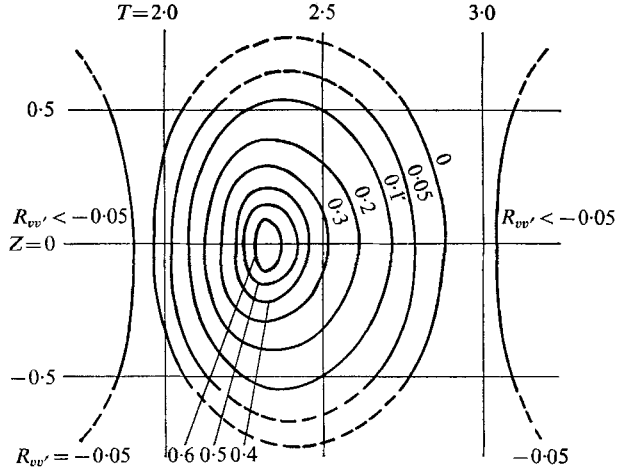

FIGURE 27. Space-time auto-correlation map of v at the half intermittency level $R_{vv'}(X_0, O, Z, T)$ at $X_0 = 2{\cdot}25$ and $y_0/\delta_0 = 0{\cdot}8$.

is responsible for the sharper and higher peaks. The lateral spread is smaller although the streamwise (T) extent is considerable.

An even more significant change in character of the turbulent burst during its downstream journey is exemplified by $R_{vI'}(X_0, O, Z, T)$, the space-time cross-correlation between the normal component v and intermittency function I shown in figure 33. Here the intermittency function I is taken from the downstream station undelayed, while the v component is taken from the upstream

probe and is delayed by T. The character of the map is similar to the one of $R_{vu'}(X_0, O, Z, T)$ given in figure 30 (except for the sign). This is reasonable to expect since I and u behave largely the same way except for their opposite signs. The other combination $R_{Iv'}(X_0, O, Z, T)$ with $X_0 = 2{\cdot}25$ and $y = 0{\cdot}5$ is shown in figure 34 and it is surprisingly different. The map is almost antisym-

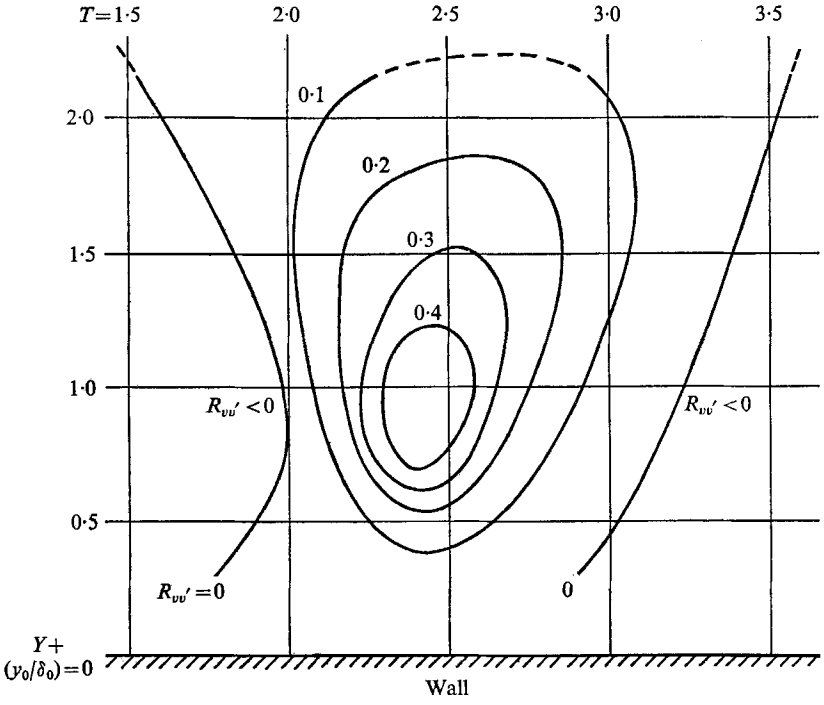

FIGURE 28. Space-time auto-correlation map of v in the normal Y–T plane $R_{vv'}(X_0, Y, O, T)$ at $X_0 = 2{\cdot}25$ and $y_0/\delta_0 = 0{\cdot}8$.

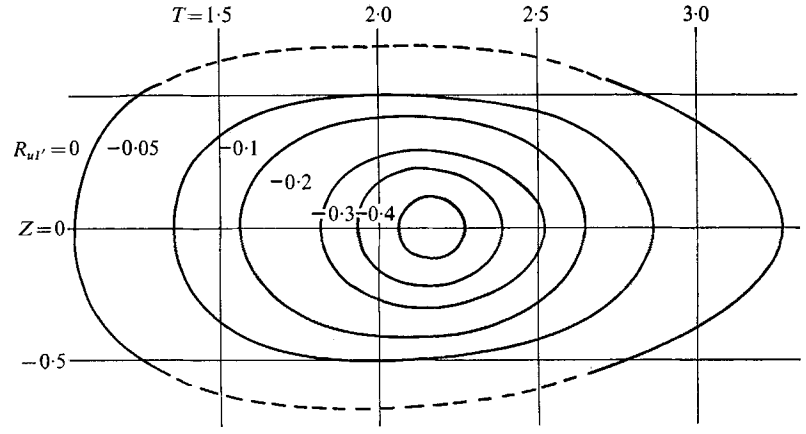

FIGURE 29. Space-time cross-correlation map of u and I at the half intermittency level $R_{uI'}(X_0, O, Z, T)$ at $X_0 = 2{\cdot}25$ and $y_0/\delta_0 = 0{\cdot}8$.

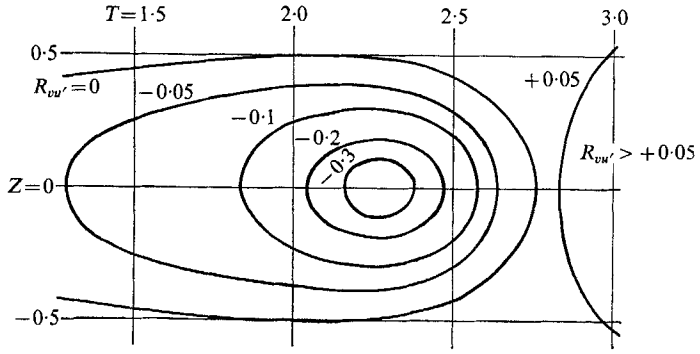

FIGURE 30. Space-time cross-correlation map at the half intermittency level of $R_{vu'}(X_0,O,Z,T)$ at $X_0 = 2{\cdot}25$ and $y_0/\delta_0 = 0{\cdot}8$. (v delayed and u taken at the downstream station.)

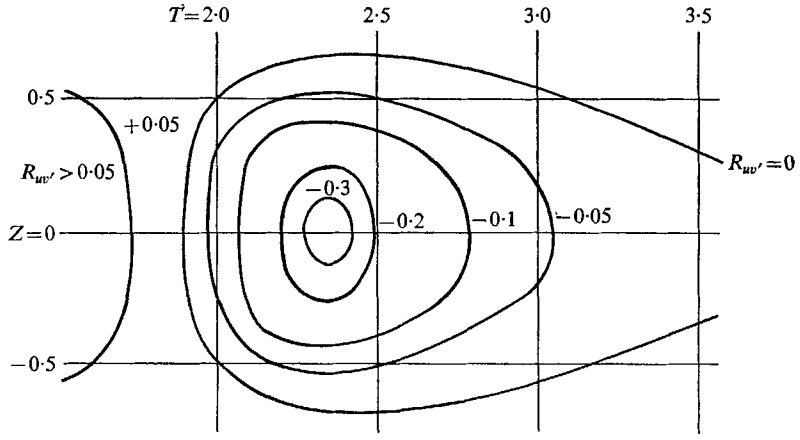

FIGURE 31. Space-time cross-correlation map at the half intermittency level of $R_{uv'}(X_0,O,Z,T)$ at $X_0 = 2{\cdot}25$ and $y_0/\delta_0 = 0{\cdot}8$. (u delayed and v taken at the downstream station.)

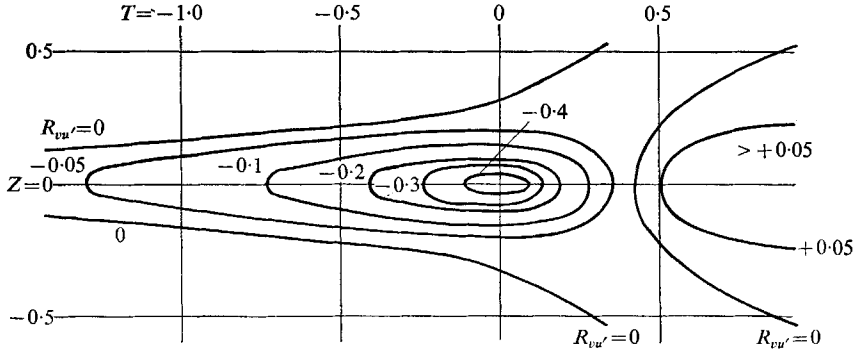

FIGURE 32. Cross-correlation map at the half intermittency level of $R_{vu'}(O,O,Z,T)$, but with no separation in the streamwise co-ordinate, with $y_0/\delta_0 = 0{\cdot}8$.

metrical around the time delay value $T = 2{\cdot}2$. In this latter case the intermittency function $I(t)$ was taken at the upstream station and first delayed, then correlated with v taken from the downstream station. The map indicates that the v component became nearly antisymmetrical with respect to the position of the turbulent burst, while at the beginning of the journey v seemed to have contained both symmetrical and antisymmetrical contributions. It is clear that many more combinations of correlations with other selected fixed values ($X_0, y_0/\delta_0$, etc.) can be measured, but one must take stock of the available data and form at least some tentative conclusion.

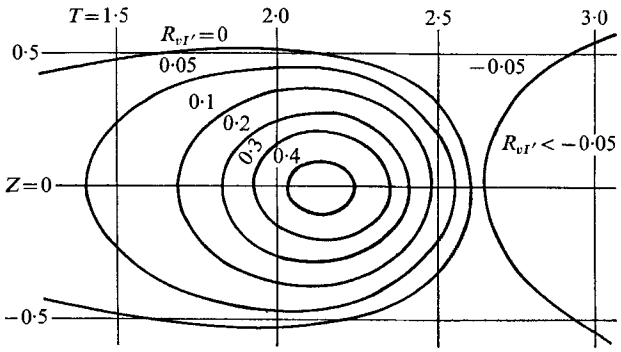

FIGURE 33. Space-time cross-correlation map at the half intermittency level of $R_{uI'}(X_0, O, Z, T)$ at $X_0 = 2{\cdot}25$ and $y_0/\delta_0 = 0{\cdot}8$. (v delayed and I taken at the downstream station.)

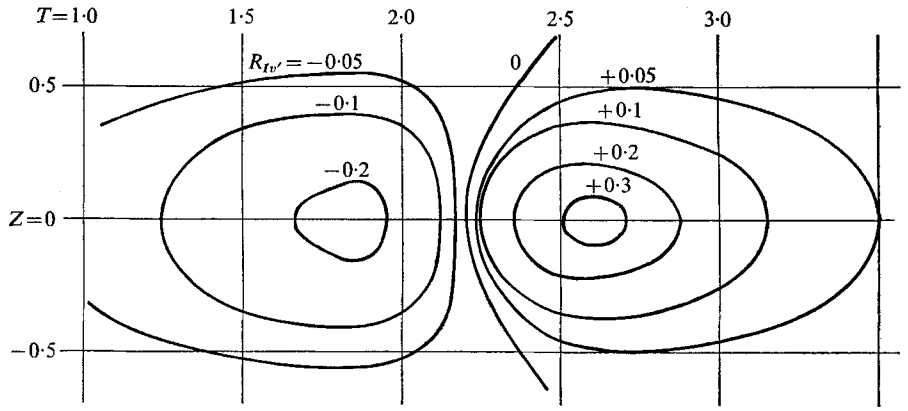

FIGURE 34. Space-time cross-correlation map at the half intermittency level of $R_{Iv'}(X_0, O, Z, T)$ at $X_0 = 2{\cdot}25$ and $y_0/\delta_0 = 0{\cdot}8$. (I delayed and v taken at the downstream station.)

6. Discussion and conclusions

The experimental results presented here clearly confirm the existence of a large scale motion strongly correlated with the shape and motion of the turbulent non-turbulent interface that separates the two clearly different types of flow regimes. The problem now is to consolidate the experimental findings into a plausible model that is consistent with all experimental data available.

The interface appears to be a highly corrugated surface with an r.m.s. slope in the X, Y plane of the order of 0·5. The individual 'bulges' or 'bursts' are strongly three dimensional; they are elongated in the streamwise direction with an aspect ratio of about 2:1; they have a typical streamwise characteristic length between $\delta/2$ and δ. This corrugated interface appears to be convected in the direction of the outside undisturbed flow, slightly lagging behind it. The outer non-turbulent flow appears to be 'riding' over the bumps or bursts of the interface. The resulting fluctuating potential flow outside the interface seems to obey Phillips' (1955) theory rather well. The observed convection velocity of the interface varies between $0{\cdot}97U_\infty$ for the 'Fronts' near the top of the bursts, and $0{\cdot}90U_\infty$ for the 'Backs' in the deep valleys, thus the length of the turbulent zone at a given y level increases continuously at a rate of about $0{\cdot}05U_\infty$.

From the space-time auto-correlation of the intermittency function, one may conclude that the individual turbulent bursts are solitary and that they occur at random. The spectrum of the intermittency function seems to corroborate this contention. If the bulges on the interface would be organized into wave packets, the correlations would show oscillations or fringes and at least some mild peaks at the preferred frequencies would occur in the spectrum of $I(t)$. It is concluded therefore that the structure of the interface can be regarded as made up of individual bursts that are similar to each other but they occur at random.

Inside the turbulent zone, the streamwise velocity decreases linearly with the distance from the interface, so there is a nearly constant rate of strain within the turbulent flow. Since the outside potential flow cannot transmit shear, the shear in the layer is maintained by continuous ejection of new bursts, resulting in the continuous growth of the turbulent region and also of the total boundary layer.

It appears that the normal velocity component V is the key to the understanding of the motion. The zone average of the normal velocity component *is* clearly positive inside the turbulent bursts and negative in the non-turbulent valleys. The maximum negative values are attained deep in the valleys where the non-turbulent fluid must be entrained into the turbulent regime. The point averages of the normal component V show in addition another type of motion. Near the interface the velocity moves away from the wall on the 'Backs' and toward the wall on the 'Fronts' and this motion is largely out of phase with the one previously described. This motion nearly follows the interface and appears to be caused by the flow 'riding' over the bursts, 'uphill' on the 'Backs' and 'downhill' on the 'Fronts'. If the shape of the turbulent bursts is visualized as a symmetrical pulse on the x, y plane, then the normal velocity V can be clearly divided into two parts, a symmetrical part and an antisymmetrical part with respect to the line of symmetry of the burst. The centre line of the burst can be identified as the line of symmetry of a square pulse in $I(t)$. In order to understand better the auto- and cross-correlations of symmetrical and antisymmetrical pulses, figure 35 was prepared. For simplicity of calculation e^{-x^2} was chosen for a symmetrical and xe^{-x^2} for an antisymmetrical pulse. The auto-correlation of a symmetrical pulse is a similar, only slightly wider pulse, showing no negative correlations. The auto-correlation of an antisymmetrical pulse is a symmetrical

pulse, but with important negative lobes on each side. Finally, the cross-correlation of the two pulse types is antisymmetrical and of course the normalized value never reaches unity. A stationary random function generated by random sprinkling of identical pulses has the same normalized auto- and cross-correlation as the respective pulses themselves by virtue of Rice's (1944) theorem.

After these remarks, we examine again figures 26, 27, 33 and 34. All four maps were prepared from data measured at the half intermittency level and they all involve the V component of the velocity. The auto-correlation in figure 26 is largely positive and it suggests rather concentrated pulses in V which is

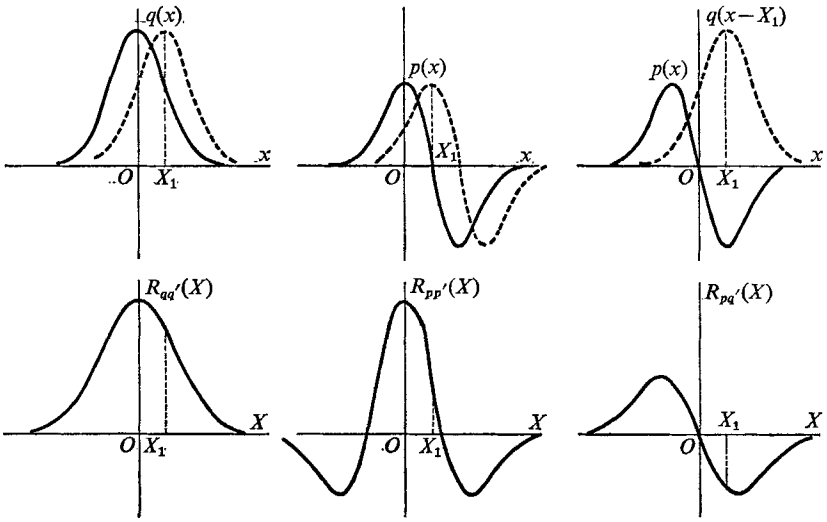

FIGURE 35. Auto- and cross-correlation of symmetrical and antisymmetrical pulses. Top: functions to be correlated. Bottom: resulting correlations.

compatible with the presence of both symmetrical and antisymmetrical components in V. After having introduced a time and a space shift, $X_0 = 2{\cdot}25$, figure 27 shows clearly the two negative lobes at the left and at the right of the main positive peak, thus suggesting the presence of a strong antisymmetric component in V. The relative development of the two component is even more striking in figures 33 and 34. First the map of $R_{vI'}$ gives the correlation of V taken at the upstream probe and then 'preserved' by the delay T to be compared with I obtained without delay at the downstream station. Clearly V contains both components, symmetrical and antisymmetrical, since the resulting map is neither symmetrical or antisymmetrical. The map of $R_{Iv'}$ is given in figure 34 and it gives the correlation of I taken at the upstream probe and 'preserved' by the delay, and then compared with the V pattern, already changed after a journey of $2{\cdot}25\delta$ that is obtained from the downstream probe. Surprisingly enough, the map in figure 34 is almost perfectly antisymmetrical around $T = 2{\cdot}2$, while figure 33 is not. This seems to indicate that the antisymmetrical component of V described above as resulting from the motion following the interface (figure 9) becomes the ultimately dominant one. On the other hand, the highly

local outward thrust that was responsible for the symmetrical part must be of short duration.

From these experimental results the following model is suggested. A new burst begins with a violent outward motion from the interior of a lump of turbulent fluid having a typical diameter of $\delta/2$. Arriving in the new environment, this lump has both a momentum defect relative to the local average velocity of the non-turbulent fluid and in addition it has also an angular momentum proportional to $\partial\overline{U}/\partial y$, characteristic of the average conditions at the level of its origin. If one could fix the co-ordinate system so that the lump at the moment of its arrival would appear as stationary, the flow of the surrounding fluid would be quite similar to the flow around a sphere. A turbulent wake would develop rapidly and it would become more and more extended in the downstream direction. This phase is of short duration, but at the same time the lump loses its momentum defect through turbulent mixing and gradually becomes the observed turbulent burst. By spreading the angular momentum over a large region, a constant $\partial\overline{U}/\partial y$ is reached within the turbulent fluid. On the other hand, the flow along the interface represents an antisymmetrical V component both outside and inside the interface, that will persist much longer during the continuing journey downstream and it gives the dominant contribution to V, but this latter antisymmetrical motion does not maintain the Reynolds stress. The experiments show that the streamwise velocity defect is quite well correlated with the presence of the bursts and it stretches over a long distance in x or t due to the 'smearing' out of the momentum defect in the individual wakes; however, the motion contributing to the Reynolds stress must be much more concentrated in space and the major contribution must come from the short, active, initial phase of the burst (see figure 32). It is conjectured that the bulges of the interface later become rather 'passive' and only the birth of new ejected lumps producing new bursts is the mechanism that maintains the Reynolds stress and thus the growth of the turbulent layer. The violent outward motion creating a new burst seems to have set up a strong potential flow reaching even outside of the boundary layer that must persist for some time as evidenced by figure 28. The localized intensive bursts reported by Kline *et al.* (1967) were clearly observed only near the viscous sublayer, so it is quite tantalizing to speculate whether or not they are responsible for the large-scale motion described here and more work in the layer near the wall will be necessary to decide it.

Finally, it may be conjectured that the large-scale wall pressure fluctuation pattern may be caused by the same mechanism and further experiments exploring that aspect would be quite valuable.

The research work reported here is a portion of a continuing programme on the structure of turbulent shear flows. Partial financial support by U.S. Army Research Office, Durham, and by U.S. Navy Office of Naval Research, is gratefully acknowledged.

Appendix

The definition of the intermittency function $I(t)$ is of course subject to certain arbitrariness. Since the detailed electronic circuit will be given elsewhere, here it is appropriate to describe the detection method only conceptually.

It was observed by Corrsin & Kistler (1955) that the turbulent vorticity fluctuations give a clearer separation between the turbulent and non-turbulent states than the velocity fluctuations. Measurement of the fluctuating vorticity, however, requires an array of four hot-wire anemometers (as given by Kistler 1952 and Kovasznay 1954). As a practical compromise the normal gradient of the streamwise velocity here $\partial u/\partial y$ was chosen as the basis of turbulence detection.

Let us define the function,

$$S(x_0, y_0, z_0, t) \equiv \frac{\partial^2 u}{\partial y\, \partial t}.$$

Experience shows that the variable $S(t)$ has relatively high fluctuations within the turbulent and relatively low fluctuations in the non-turbulent regime. An *a posteriori* justification is given in figure 15. The spatial differentiation with respect to y was performed by placing two closely spaced parallel wires and then obtaining the difference of their linearized output; temporal differentiation was accomplished by an analogue circuit.

In order to develop a satisfactory criterion for detection, a minimum of two adjustable parameters are required. One regards the $S(t)$ signal as the signal to be 'detected' in the presence of 'noise', since the 'parasitic' value of $S(t)$ during the non-turbulent intervals may be regarded as unwanted 'noise'. One of the two parameters is essentially a threshold value C chosen at a suitable level so that the smaller fluctuations will be classed as non-turbulent and larger fluctuations as turbulent. The other parameter is an integrating or averaging time constant called here the 'hold-time' τ_H that represents the length of time intervals during which the threshhold criterion is applied. Clearly the threshold level C and the holding time τ_H must be chosen according to the properties of the turbulent fluctuations. As far as the properties of the turbulent regime in the intermittent zone are concerned, one may choose as a first approximation the turbulent properties in the interior of the boundary layer where the intermittency has reached the value $\gamma = 1$. Here one may define a characteristic frequency f_{ch} or the characteristic time T_{ch} of the turbulent fluctuations by simply comparing the r.m.s. value of S and its time derivative $\dot{S} = \partial S/\partial t$,

$$\frac{\overline{\dot{S}^2}}{\overline{S^2}} = 4\pi^2 f_{ch}^2 = \frac{4\pi^2}{T_{ch}^2}. \tag{A 1}$$

The detection process was based on the instantaneous absolute magnitude values of S and $\dot{S}$. First an intermediate function $H(t)$ was determined:

$$H(t) = \begin{cases} 0 & \text{when} \quad |S| < C \quad \text{and} \quad |\dot{S}| < 2\pi f_{ch} C, \\ 1 & \text{when} \quad |S| \geqslant C \quad \text{or} \quad |\dot{S}| \geqslant 2\pi f_{ch} C. \end{cases}$$

The threshold value for $\dot{S}$ was chosen proportional to f_{ch} based on dimensional reasoning. The above definition amounts to the statement that $H = 1$ whenever the instantaneous absolute value of either the function of S or its time derivative S exceeds a prescribed limit. The function $H(t)$ depends only on the instantaneous values and therefore would not be suitable to serve as the intermittency function $I(t)$. Since S and $\dot{S}$ are both fluctuating quantities, there will be momentary lapses when both will be below the required threshold. At these moments, $H = 0$ and non-turbulent flow would be indicated. Conversely, momentary large excursions may also occur during the non-turbulent intervals; these are due to the large short duration excursions in the 'noise'. In order to avoid a large number of these 'false alarms', a certain smoothing is required. This is carried out in two steps. First, a smoothed function $J(t)$ is formed

$$J(t) = \frac{1}{\tau}\int_{-\infty}^{t} H(t')e^{(t'-t)/\tau}\,dt'.$$

$J(t)$ is a continuous function of t. The intermittency function $I(t)$ now can be defined:

$$I(t) = \begin{cases} 1 & \text{when} \quad J(t) \geqslant \frac{1}{2}, \\ 0 & \text{when} \quad J(t) < \frac{1}{2}. \end{cases}$$

Clearly the exponentially weighted integration over the past record of $H(t)$ introduces a time lag, $\tau_H = \tau \ln 2 \approx 0{\cdot}7\tau$ into the detection; but, on the other hand, isolated, very short duration pulses fail to satisfy the threshold requirements and will not change the state of $I(t)$ and increase $f\gamma$.

The two parameters C and τ_H are of course arbitrary, at least in principle, but reasonable choices can be made. The threshold C must be chosen somewhere between the turbulent and the non-turbulent r.m.s. signal level. A reasonably well-defined choice can be made

$$C = (S'_T S'_{NT})^{\frac{1}{2}},$$

where S'_T is the r.m.s. level of S in the turbulent and S'_{NT} in the non-turbulent regime. *A posteriori* one find that $S'_T = \tilde{\tilde{S}}'$ and $S'_{NT} = \tilde{\tilde{S}}'$. First one assumes a value for C, then by determining $\tilde{\tilde{S}}'$ and $\tilde{\tilde{S}}'$ it is possible to iterate.

The detection method of course improves with increasing S_T/S_{NT}, which can be regarded as the 'signal-to-noise' ratio of the detection (see figure 15).

The other parameter τ_H must be chosen proportional to T_{ch}, the characteristic time scale of the turbulence. A reasonable first choice is $\tau_H = T_{ch}/2$ and this was used throughout the measurements reported in this paper. The actual choice of this parameter is slightly influenced by the ratio of the characteristic frequency f_{ch} to the intermittency frequency f_γ. The frequency f_γ scales proportional to free-stream velocity and inversely proportional to the thickness of the boundary layer. The characteristic frequency f_{ch} scales roughly inversely proportional to λ, the dissipation scale or microscale. The ratio of these two time scales increases with increasing Reynolds number of the boundary layer.

REFERENCES

BRADBURY, L. J. S. 1965 *J. Fluid Mech.* **23**, 31.

BRADSHAW, P. 1967 *J. Fluid Mech.* **27**, 209.

CLAUSER, F. H. 1954 *J. Aero. Sci.* **21**, 91.

CORRSIN, S. 1943 *NACA Wartime Rep.* W-94.

CORRSIN, S. & KISTLER, A. L. 1955 *NACA Rep.* 1244.

FAVRE, A., GAVIGLIO, J. & DUMAS, R. 1957 *J. Fluid Mech.* **2**, 313.

FAVRE, A., GAVIGLIO, J. & DUMAS, R. 1958 *J. Fluid Mech.* **3**, 344.

FAVRE, A., GAVIGLIO, J. & DUMAS, R. 1967 *Phys. Fluids*, **10**, S138.

FIEDLER, H. & HEAD, H. R. 1966 *J. Fluid Mech.* **25**, 719.

IMAKI, K. 1968 *Bull. Inst. Space and Aero. Sci., University of Tokyo*, Part I **4**, 448; Part II **4**, 536 (in Japanese only).

KAPLAN, R. E. & LAUFER, J. 1968 *Proc. 12th Int. Congress Mech.* (to be published).

KIBENS, V. 1968 Ph.D. Dissertation, The Johns Hopkins University.

KISTLER, A. L. 1952 M.S. Thesis, The Johns Hopkins University.

KLEBANOFF, P. S. 1954 *NACA Rep.* 1247.

KLINE, S. J., REYNOLDS, W. C., SCHRAUB, R. A. & RUNDSTADLER, P. W. 1967 *J. Fluid Mech.* **30**, 747.

KOVASZNAY, L. S. G. 1954 Turbulence measurements. *High Speed Aerodynamics and Jet Propulsion*, **10**, 227. Princeton University Press.

KOVASZNAY, L. S. G., KOMODA, H. & VASUDEVA, B. R. 1962 *Proc. Heat. Transf. and Fluid Mech. Inst.* Stanford University Press.

KOVASZNAY, L. S. G., MILLER, L. T. & VASUDEVA, B. R. 1963 *Project SQUID Tech. Rep.* JHU-22-P.

KOVASZNAY, L. S. G. & CHEVRAY, R. 1969 *Rev. Sci. Instr.* **40**, 91.

LIEPMANN, H. W. 1954 *GALCIT/NACA Rep. NAW*-6288.

NEE, V. W. & KOVASZNAY, L. S. G. 1969 *Phys. Fluids*, **12**, 473.

PHILLIPS, O. M. 1955 *Proc. Camb. Phil. Soc.* **51**, 220.

RICE, O. 1944 *Bell Syst. Tech. J.* **23**, 282.

RICE, O. 1945 *Bell Syst. Tech. J.* **24**, 46.

ROSHKO, A. 1953 *NACA TN* 2913.

STEWART, R. W. 1956 *J. Fluid Mech.* **1**, 593.

TOWNSEND, A. A. 1949 *Austr. J. Sci. Res.* Ser. A **2**, 451.

TOWNSEND, A. A. 1966 *J. Fluid Mech.* **26**, 689.

TRITTON, D. J. 1959 *J. Fluid Mech.* **6**, 547.

TRITTON, D. J. 1967 *J. Fluid Mech.* **28**, 439.